

# Sensing Out-of-Equilibrium and Quantum Non-Gaussian environments via induced Time-Reversal Symmetry Breaking on the quantum-probe dynamics

Martin Kuffer,<sup>1,2,3</sup> Analía Zwick,<sup>1,2,3</sup> and Gonzalo A. Álvarez<sup>1,2,3,\*</sup>

<sup>1</sup>*Centro Atómico Bariloche, CONICET, CNEA, S. C. de Bariloche, 8400, Argentina*

<sup>2</sup>*Instituto de Nanociencia y Nanotecnología, CNEA, CONICET, S. C. de Bariloche, 8400, Argentina*

<sup>3</sup>*Instituto Balseiro, CNEA, Universidad Nacional de Cuyo, S. C. de Bariloche, 8400, Argentina*

Advancing quantum sensing tools for investigating systems at atomic and nanoscales is crucial for the progress of quantum technologies. While numerous protocols employ quantum probes to extract information from stationary or weakly coupled environments, the challenges intensify at atomic- and nano-scales where the environment is inherently out-of-equilibrium or strongly coupled with the sensor. We here prove that the time-reversal symmetry in the quantum-sensor control dynamics is broken, when partial information is probed from an environment that is out-of-equilibrium with non-stationary fluctuations or is described by quantum non-Gaussian, strongly coupled environmental correlations. We exploit this phenomenon as a quantum sensing paradigm with proof-of-principle experimental quantum simulations using solid-state nuclear magnetic resonance (NMR). This introduces a signal contrast on a qubit-probe that quantifies how far the sensed environment is from equilibrium or its quantum non-Gaussian nature. Protocols are also presented to discern and filter a variety of environmental properties including stationary, non-stationary and non-Gaussian quantum noise fluctuations as a step toward sensing the ubiquitous environments of a quantum-sensor at atomic and nanoscales.

## I. INTRODUCTION

The progress on controlling single quantum systems at atomic and nanometric scales has lead to the development of quantum technologies [1–3]. Both the storage and processing of quantum information in quantum devices suffer from decoherence, the loss of quantum information as a function of time, that distorts the encoded information [4]. Nevertheless, decoherence effects are a key information resource about the environment that is exploited for designing novel quantum sensors with important applications in geology, archaeology, material science, biology and medicine [5–7].

These quantum probes have strong potential to enable measurement of physical properties with unprecedented sensitivity, but more importantly they allow probing spatial scales that are not accessible by classical means, such as the atomic and nanoscales [5, 6]. They have already enabled the magnetometry of single neurons [8] and magnetic biomarkers with subcellular resolution [9], microscale and nanoscale detection of single molecules [10, 11], and the probing of temperature-dependent biological processes in cells and small organisms [12].

In the context of these scales, particularly when employing single quantum sensors, environmental systems either manifest intrinsic out-of-equilibrium features or can be unavoidable driven out-of-equilibrium via the quantum feedback induced by the probe, both inducing non-stationary environmental fluctuations [13–18]. Moreover, quantum probes at these scales can be strongly coupled to its environment generating what is known as non-Gaussian effects [19–25]. Conventional frameworks to describe the quantum open nature of these sensors do not account for non-stationary environmental features and/or non-Gaussian ef-

fects [4, 5, 26, 27]. Only recently, due to progress in quantum sensing technologies, frameworks for sensing out-of-equilibrium and/or non-Gaussian environments with quantum sensors have been introduced [17, 18, 20, 21, 23–25].

In this article, we delve into the realm of time reversal symmetry to design quantum control sensing-paradigms of the ubiquitous environments found at atomic and nanoscales. We demonstrate the time reversal symmetry breaking in the quantum control of a qubit-sensor, specifically when coupled to quantum non-Gaussian and/or out-of-equilibrium environmental interactions. Leveraging this characteristic, arising from the partial information observed by a quantum-probe, we present a novel quantum sensing paradigm rooted in the design of time-asymmetric dynamical control of the sensor. We name this technique SENSIT (Sensing of Environmental Non-Symmetric Information due to T-symmetry breaking) and demonstrate it through experimental quantum simulations using solid-state NMR.

In this context, we illustrate how the distance of the quantum environmental state from equilibrium can be encoded onto a qubit-probe signal contrast. Furthermore, we showcase the selective filtration of non-stationary features with respect to stationary noise fluctuations. Additionally, we introduce protocols that leverage this contrast to selectively quantify quantum non-Gaussian features and non-equilibrium characteristics of the environment. Overall, our work marks a step forward in the practical application of quantum sensing technology, offering valuable insights into the ubiquitous out-of-equilibrium and quantum non-Gaussian environments encountered by quantum sensors.

## II. DECODING ENVIRONMENTAL INFORMATION THROUGH DYNAMICALLY CONTROLLED QUBIT-SENSOR

To demonstrate the quantum sensing paradigm based on the time reversal symmetry breaking, we consider a dynamically controlled qubit-sensor coupled to an environment that induces pure dephasing. This quantum sensor platform is found in a variety of systems as in electrons in diamonds [11, 28, 29], electronic spins in nanoscale nuclear spin baths [30], quantum dots [31], donors in silicon [32], superconducting qubits [27], trapped atoms [33], and solid-, liquid- and gas-state NMR systems [7, 26].

Control on the qubit-sensor via dynamical decoupling effectively modulates the strength of the qubit-environment interaction and can thus be used to selectively encode environmental information on the signal decay of the qubit-sensor [26, 27]. In the interaction picture with respect to the environmental evolution and control of the qubit, the qubit-environment Hamiltonian is

$$H_{SE}(t) = f(t)S_z B(t), \quad (1)$$

where  $S_z$  is the qubit-probe spin operator in the  $z$  direction,  $B(t)$  is the noise operator representing the environmental fluctuating degrees of freedom that induce dephasing on the qubit-probe, and  $f(t)$  is the qubit-environment interaction whose time dependence is only due to the modulation induced by dynamical decoupling [26, 27, 34–37] (Fig. 1a). The fluctuating noise operator is given by  $B(t) = e^{iH_E t} B e^{-iH_E t}$ , where  $H_E$  is the environmental Hamiltonian and  $B$  is the environmental degree of freedom coupled to the qubit-probe.

The evolution operator of the qubit-probe is thus  $U(T_s) = \mathcal{T} e^{-i \int_0^{T_s} dt f(t) S_z B(t)}$ , where  $\mathcal{T}$  is the time-order superoperator and  $T_s$  is the sensing time, the time during which the qubit-sensor dephases due to sensing the environmental fluctuations. The probe observable is the in-plane qubit-polarization that decays as  $M(T_s) = \frac{\langle S_+ \otimes \mathbb{I}_E \rho(T_s) \rangle}{\langle S_+ \otimes \mathbb{I}_E \rho(0) \rangle} = e^{-\mathcal{J}(T_s)}$  due to the environment with the decoherence factor  $\mathcal{J}$ , where  $\rho(T_s)$  is the density matrix of the full qubit-environment system after the qubit has sensed the environment,  $\langle \cdot \rangle = \text{tr}[\cdot]$ , and  $S_+ = S_x + iS_y$  the up spin operator.

We assume that, in the quantum sensing protocol, the qubit-environment system is initially in a separable state when the probe is brought into contact with the environment. Specifically, we consider the initial state  $\rho(0) = \rho_0 = p S_x \otimes \rho_E$  with the qubit polarized in the  $x$  direction. We do not explicitly write terms proportional to the qubit identity  $\mathbb{I}_S$  in the density matrix, as they do not contribute to the qubit-probe signal.

We perform a cumulant expansion of the decoherence factor  $\mathcal{J}$  on the SE interaction coupling strength with the environment

$$\mathcal{J}(T_s) = - \sum_n \frac{i^n}{n!} \int_0^{T_s} dt_1 \cdots \int_0^{T_s} dt_n f(t_1) \cdots f(t_n) W_n(t_1, \dots, t_n) \quad (2)$$

where  $W_n$  are the cumulants that completely characterize the environment fluctuations felt by the qubit-sensor. They are defined based on the environmental correlation functions

$$G_n(t_1, \dots, t_n) = \frac{1}{2^{n-1}} \langle \{B(t_1), \{B(t_2), \{\dots, B(t_n)\} \dots\} \} \rho_E \rangle \quad (3)$$

for  $t_1 \leq t_2 \leq \dots \leq t_n$  with  $\{\cdot, \cdot\}$  the anti-commutator (see SI A).

## III. ENVIRONMENT-INDUCED TIME-REVERSAL SYMMETRY BREAKING

In quantum mechanics, the evolution operator  $U(t)$  is unitary, meaning it is invertible ( $U^\dagger(t) = U^{-1}(t)$ ). When a quantum system exhibits time-reversal symmetry, this is typically expressed through the time reversal operator  $T$ , which is an anti-unitary operator. Time reversal symmetry implies that  $T$  commutes with the system Hamiltonian  $[T, H] = 0$  and thus satisfies  $T^{-1}U(t)T = U^{-1}(t)$  [38].

At first glance, one might expect this symmetry to result in a corresponding symmetry on the control operation of the qubit-probe dynamics. However, we here demonstrate that when a dynamically controlled qubit-sensor probes an environment, the partial information accessible to the sensor, obtained through the partial trace of environmental degrees of freedom, can unveil a breaking in the time-reversal symmetry of the control function. In particular, we illustrate that the symmetry is disrupted, when the noise operators of the environment, denoted as  $B(t)$ , fail to commute at different times. This breakdown occurs explicitly when the decoherence factor involves cumulants of order  $n \geq 3$ . Moreover, we also show that the symmetry is always broken if the environmental fluctuations are non-stationary, indicative of non-equilibrium features (Proof in SI C).

Quantum non-Gaussian noises thus induce time-reversal symmetry breaking in the quantum control of the qubit-sensor. These noises are characteristic of quantum environments strongly coupled to the sensor and operating at low temperatures. The manifestation of symmetry breaking is absent when the environment is weakly coupled validating the Gaussian approximation, or at the high-temperature limit leading to the semiclassical field approximation (see SI C 2). Furthermore, in the latter scenario, if the environmental fluctuations are non-Gaussian but can be effectively described by classical fields, the time-reversal symmetry remains protected.

A nonstationary environment does not have cumulants invariant under time translation  $\Delta t$ , i.e.  $W_n(t_1, \dots, t_n) \neq W_n(t_1 + \Delta t, \dots, t_n + \Delta t)$ . In this case, for quantum or classical noise operators, the time-reversal symmetry of the control is broken. Notice that time translation symmetry is achieved when the environment reaches a stationary state, including when it is in equilibrium. This is illustrated in

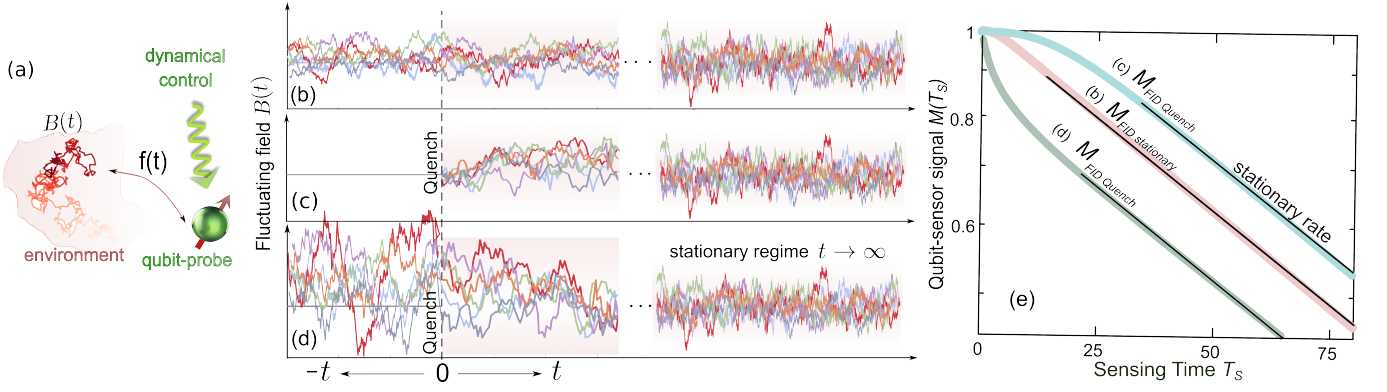


Figure 1. (a) Schematic illustration of the dynamically modulated interaction  $f(t)$ , enabling the qubit-probe to sense its environment. Realizations of a stochastic process of (b) a stationary fluctuating field  $B(t)$  as a function of time and (c,d) stochastic processes representing an out-of-equilibrium environment due to a quench by a change in the dynamics of the process at  $t = 0$ . In (c), prior to  $t = 0$ , the fluctuating field remains fixed at 0, evolving stochastically for  $t \geq 0$  and reaching a stationary regime for  $t \rightarrow \infty$ . Notably, around  $t \sim 0$ , the field exhibits a smaller variance than at equilibrium, resulting in a comparatively less impact of the qubit control on its signal. In (d) preceding  $t = 0$ , the fluctuating field has a greater variance than for  $t \rightarrow \infty$ , evolving stochastically for  $t \geq 0$  and attaining a stationary regime for  $t \rightarrow \infty$ . Around  $t \sim 0$ , the field has a greater variance than at equilibrium, leading to a more pronounced impact of the qubit control on its signal compared to the equilibrium state. (e) Qubit-sensor signal  $M(T_s)$  as a function of the sensing time  $T_s$  for the fluctuating field displayed in panels (b-d). Distinctions emerge at shorter times, yet the signals converge to the same decay rate upon reaching the stationary regime. The decay-shift from the stationary curve reflects the influence of an out-of-equilibrium environment during the earlier times.

Fig. 1, which compares stationary fluctuations of the field  $B(t)$  (panel b) with non-stationary fluctuations induced by quenches (panels c and d). Time-reversal symmetry—in the control—is broken in the latter cases.

This asymmetry in time evolution is reflected in the dephasing of the qubit-probe (Fig. 1e), where the dephasing near the quench decays slower or faster compared to the stationary case, depending on whether the noise fluctuation variance just before the quench is lower or higher than in the stationary regime. This exemplifies how one can exploit the manifestation of the time reversal symmetry breaking of the environment on the qubit-probe dephasing.

The qubit-probe signal has time-reversal symmetry in the control function if the cumulants in Eq. (2) satisfy the symmetry condition  $W_n(t_1, \dots, t_n) = (\pm 1)^n W_n(T_s - t_1, \dots, T_s - t_n)$ . The sign  $(\pm 1)^n$  depends on the nature of the noise, i.e. when the noise operator  $B$  is an electric charge, electric field, gate potential, etc. the sign corresponds to 1, and in cases where it is a magnetic field, magnetization, electric current, etc. corresponds to  $-1$ . We thus call these cases of the electric- and magnetic-type, respectively (details and proof in SI C2). The cumulants exhibit this symmetry if and only if they possess time translation symmetry, and the noise operators commute at different times or their non-commutation is negligible.

Under these conditions, we prove that the qubit-probe signal satisfies time-reversal symmetry in the control function

$$M_f = e^{-\mathcal{J}_f} = \begin{cases} M_{f_T} = e^{-\mathcal{J}_{f_T}} & \text{electric-type} \\ M_{f_T}^* = e^{-\mathcal{J}_{f_T}^*} & \text{magnetic-type} \end{cases}, \quad (4)$$

where  $M_f$  is the signal measured when using the control function  $f$  and  $M_{f_T}$  is that measured when using as control the time reversal of  $f$ , i.e.  $f_T(t) = f(T_s - t)$  (proof in SI C3). This demonstrates that the polarization of the qubit-probe remains invariant, up to conjugation, under time reversal of the control sequence determined by the control function  $f$ , when the cumulants exhibit time-reversal symmetry. This time-reversal symmetry is a consequence of stationary correlation functions of an environment plus negligible quantum noncommutativity effects guaranteed only by classical fields, weak coupling, high temperature or Gaussianity. When either of these conditions fails, the symmetry is broken, thus enabling the measurement of quantum non-Gaussianity and/or non-stationary phenomena due to out-of-equilibrium dynamics.

Therefore the argument  $\Delta \mathcal{J} = \mathcal{J}_f - \mathcal{J}_{f_T}^{(*)}$  of the ratio between the corresponding qubit-probe signals  $M_f/M_{f_T}^{(*)} = \exp\{-\Delta \mathcal{J}\}$  is proportional to the degree of environmental time-reversal symmetry breaking and/or the breaking of the time translation symmetry of the environmental correlation functions (see SI B and C). Here  $(*)$  corresponds to the complex conjugation applied only for magnetic-type cases. The ratio  $M_f/M_{f_T}^{(*)}$  is in general a complex number, where its modulus is given by the even cumulants and the phase by the odd cumulants (see SI C3). Thus the modulus defines the *SENSIT qubit-signal contrast*, and the phase, the *SENSIT qubit-phase contrast* (see SI B). In this article, our emphasis is on the *SENSIT qubit-signal contrast* due to its greater accessibility and robustness in experiments. However, in principle, either

quantity can be employed.

The SENSIT qubit-signal contrast is

$$\text{Re}\Delta\mathcal{J} = - \sum_{n=0}^{\infty} \frac{(-1)^n}{(2n)!} \int_0^{T_s} dt_1 f(t_1) \cdots \int_0^{T_s} dt_{2n} f(t_{2n}) \Delta W_{2n}(t_1, \dots, t_{2n}), \quad (5)$$

where

$$\Delta W_{2n}(t_1, \dots, t_{2n}) = W_{2n}(t_1, \dots, t_{2n}) - W_{2n}(T_s - t_1, \dots, T_s - t_{2n}) \quad (6)$$

is the difference between the  $2n$ -th cumulant at forward times  $t_i$  and at the time reversed ones from the sensing time  $T_s - t_i$ . These quantities serve as order parameters, gauging the extent of time-reversal symmetry breaking in the qubit-control. The SENSIT contrast, therefore, acts as a probe for these order parameters, with weights determined by the control function  $f(t)$ . Notice that in Eq. (5), we performed a change in the time variables to convert the reversed control  $f_T(t)$  into  $f(t)$ , and this change the arrow of time in the cumulants  $W_{2n}(T_s - t_1, \dots, T_s - t_{2n})$ .

The key to utilizing this quantification lies in its resilience against any noise contribution to qubit-probe dephasing that does not induce a time-reversal symmetry breaking, i.e. a contribution that is stationary and such that the noise operators either commute at different times or their non-commutation is negligible. This robustness is ensured as the terms from  $W_{2n}(t_1, \dots, t_{2n})$  cancel out with those in  $W_{2n}(T_s - t_1, \dots, T_s - t_{2n})$  and similarly for the phase term (proof in SI C3). This means that if the sensed environment can be separated into two independent parts,  $a$  and  $b$ , such that only  $a$  induces a time-reversal symmetry breaking on the control, then the SENSIT contrast will exclusively sense properties of  $a$ ; while remaining completely independent of  $b$ . Consequently, the SENSIT contrast exclusively responds to noise sources that induce the time-reversal symmetry breaking of the qubit-probe control (SI D). This may set an avenue for pump and probe experiments, where a qubit that interacts with a complex environment is used to sense just a part of it by first driving the desired target subsystem out of equilibrium (pump) and then use SENSIT to selectively detect just that subsystem (probe).

To give an example, the SENSIT contrast provides information about the distance to equilibrium. In the simple but general case when the environment state  $\rho_E = \rho_E^{(0)} + \epsilon \rho_E^{(1)}$  is near to a stationary state  $\rho_E^{(0)}$ , with  $\rho_E^{(1)}$  a constant perturbation, we demonstrate that  $\Delta\mathcal{J} \propto \epsilon$  thus quantifying the distance to equilibrium (see SI E). In the particular cases illustrated in Fig. 1, the SENSIT contrast  $\text{Re}\Delta\mathcal{J} \propto (\sigma - \sigma_0)$ , where  $\sigma$  the variance of the noise fluctuation before the quench, and  $\sigma_0$  the variance at the stationary regime achieved at long times after the quench (see SI F). This thus sets a paradigmatic example about

how the SENSIT contrast is proportional to the distance  $(\sigma - \sigma_0)$  of the initial state of the environment to its stationary state at equilibrium.

#### IV. EXPERIMENTAL DETECTION OF OUT-OF-EQUILIBRIUM STATES

One of our main results is that the SENSIT contrast, being a readily available quantity in experimental setups, serves as a sensing protocol for detecting and characterizing out-of-equilibrium and/or quantum non-Gaussian environments. To provide a concrete illustration of the underlying principles of SENSIT and enhance the clarity of the introduced general results, we experimentally performed solid-state NMR quantum simulations on a Bruker Avance III HD 9.4T WB NMR spectrometer with a  $^1\text{H}$  resonance frequency of 400.15 MHz and a  $^{13}\text{C}$  resonance frequency of 100.61 MHz. The  $^{13}\text{C}$  nucleus plays the role of the qubit-probe, and the surrounding  $^1\text{H}$  nuclei are considered the environment. Since  $^{13}\text{C}$  is in natural abundance, it is present in low concentration and all interaction between  $^{13}\text{C}$  nuclei are negligible on the performed experiments (see SI G1 for details on the experimental setup).

The system is initially in thermal equilibrium, as represented in the first step of the sensing protocol in Fig. 2a. We induce an out-of-equilibrium state in the environment to generate non-stationary noise fluctuations on the qubit-sensor. To achieve this, we initially employ the qubit-probe to build up quantum correlations between the qubit and the environmental spins during a preparation time  $T_p$ , ensuring a localized spread of information near the sensor (Fig. 2a,b). Then we performed a quantum nondemolition measurement on the qubit-probe state mimicked by induced dephasing to erase the probe-environment correlations [7, 39]. This procedure leaves the environment in a correlated out-of-equilibrium state (see third step of Fig. 2a and SI G2). All these steps constitute the preparation of a nonequilibrium state in the environment.

Subsequently, we initialize the qubit-probe state in a separable state with the environment  $\rho_0 = p S_x \otimes \rho_E$  by the application of a  $\pi/2$  pulse on the qubit. After the initialization, we proceed to implement non-equidistant dynamical decoupling sequences to manipulate the time-reversal symmetry of the sequence. We observe the decay of the qubit signal at the sensing time  $T_s$ , representing the duration of the dynamical decoupling sequence, to quantify the SENSIT contrast. This process is illustrated in the last two steps



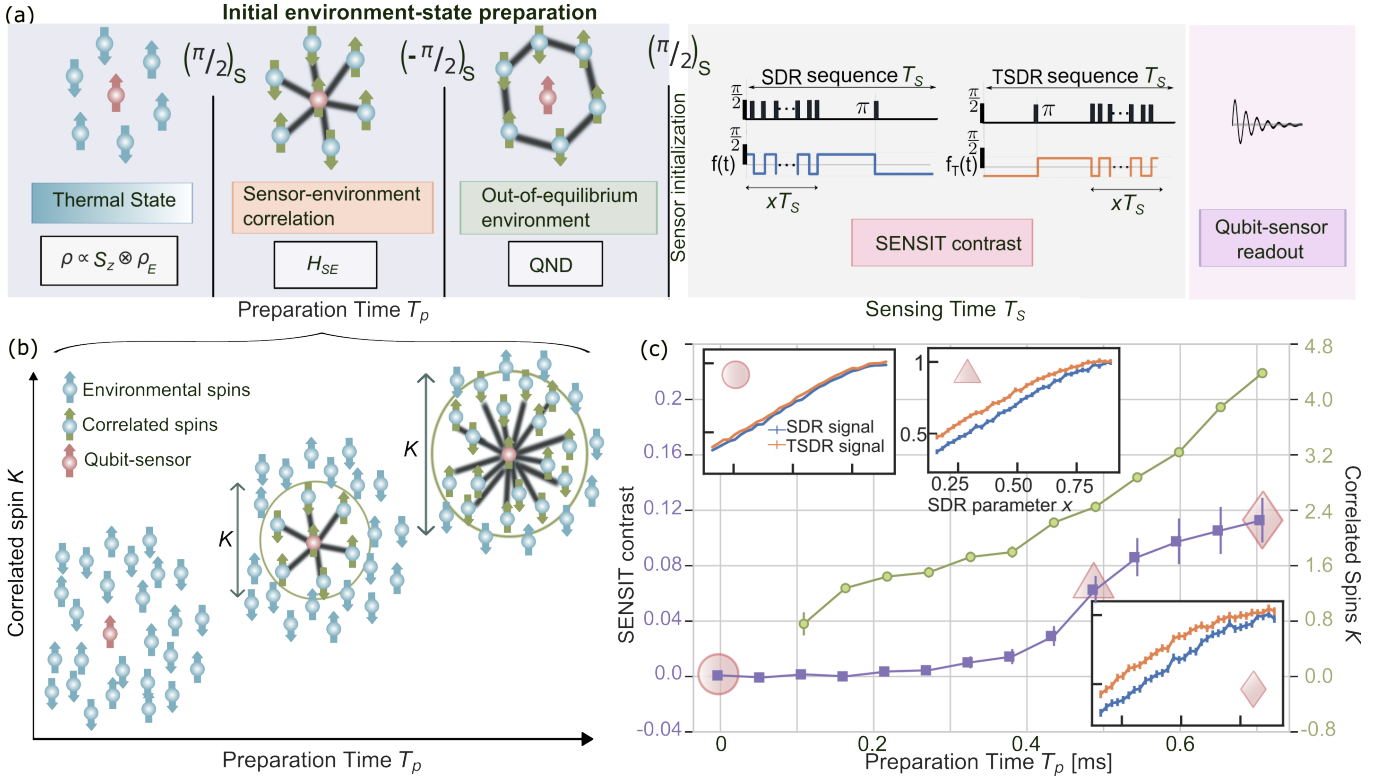


Figure 2. Illustration of nonequilibrium sensing with SENSIT. (a) Experimental protocol diagram implemented to induce nonequilibrium in the qubit environment and its detection using the SENSIT technique. (b) Schematic representation of the out-of-time-order commutator  $K$ , a well-established measure quantifying the correlation of environmental spins with the qubit during preparation. (c) Correlated spins  $K$  and SENSIT contrast, measured by the qubit, as a function of the preparation time  $T_p$ . Error bars for  $K$  are obtained from a fit, while those for the SENSIT contrast account for the NMR detection sensitivity. The SENSIT contrast  $\int_0^{\frac{N-1}{N}} dx \text{Re} \Delta \mathcal{J}(x)$  quantifies the environmental non-equilibrium degree by integrating the difference of  $\text{Re} \Delta \mathcal{J}(x)$  between SDR and TSDR sequences over the parameter  $x$ . Insets show the signals measured by SDR and TSDR control sequences for various preparation times (indicated by geometrical symbols). Using  $N = 12$  pulses in our experiments, the curves match at equilibrium ( $T_p = 0$ ), and diverge as the environment deviates from equilibrium. This experimental demonstration highlights the utilization of time-reversal symmetry breaking for measuring nonequilibrium environments.

of Fig. 2a.

We employed the Selective Dynamical Recoupling (SDR) sequence [40, 41], chosen for its simplicity in constructing a time-asymmetric sequence using only  $\pi$ -pulses, along with the flexibility of having a single parameter that can be adjusted without changing  $T_s$ . This makes SDR the most straightforward choice for our purposes. It consists of a concatenation of a CPMG spin-echo train with  $N - 1$  rapid, spin-echo train  $\pi$ -pulses between the times  $t = 0$  and  $t = xT_s$ , and a Hahn spin-echo sequence consisting of a single echo  $\pi$ -pulse at the center between the times  $xT_s$  and  $T_s$ . The SDR modulation  $f(t)$  is shown with the blue curve in Fig. 2a. Here  $x$  is a dimensionless parameter, that defines the asymmetry of the SDR sequence interpolating between a single Hahn echo at  $x = 0$  and a CPMG sequence of  $N$  equidistant pulses at  $x = \frac{N-1}{N}$ . The time-reversed SDR (TSDR) sequence contains the inverse succession in time of the  $\pi$ -pulses, consisting first of the single Hahn-echo sequence between times 0 and  $(1 - x)T_s$ ,

followed by the  $N - 1$  CPMG pulses between the times  $(1 - x)T_s$  and  $T_s$  (see the orange curve for  $f_T(t)$  in Fig. 2a and SI G2).

The insets in Fig. 2c illustrate the qubit-probe signal following the SDR and TSDR modulations as a function of  $x$ , for a fixed total sensing time and varying preparation times  $T_p$  for the initial out-of-equilibrium state in the environment. The results demonstrate that the SDR and TSDR signals are indistinguishable at  $T_p = 0$  when the environment is stationary at equilibrium. Subsequently, they showcase how the signals progressively increase their contrast as the environment is shifted further out of equilibrium producing non-stationary noise fluctuations.

To get a single SENSIT-contrast quantification of the non-equilibrium degree of the environmental state, we integrate the attenuation factors of the qubit signals  $\int_0^{\frac{N-1}{N}} dx \text{Re} \Delta \mathcal{J}(x)$  over the parameter  $x$  (main panel of Fig. 2c). This contrast is proportional to the distance of the initial environmental state from equilibrium, conse-

quently increasing as a function of the preparation time, with a greater number of environmental spins becoming correlated (see SI C).

These experiments were performed at room temperature that represents a high-temperature limit as the thermal energy is much larger than the Zeeman energy of the spins (see SI G 1), therefore the time-reversal symmetry for quantum control described in Eq. (4) will only be broken if the environment is out-of-equilibrium manifesting non-stationary noise fluctuations. Thus here we demonstrate how the SENSIT contrast probes a quenched state on the environment and determines how far from equilibrium it is [13, 24, 25].

## V. COMPARING SENSIT CONTRAST AND OUT-OF-TIME-ORDER CORRELATION METRICS FOR OUT-OF-EQUILIBRIUM STATES

To have an alternative method for quantifying the out-of-equilibrium degree, we employed a more established approach based on out-of-time-order correlations (OTOC) measured with multiple quantum coherences [15, 42]. This method assesses the non-commutation degree of the evolved density matrix during the preparation time in relation to the initial state of the environment before preparation, as depicted in Fig. 2b. This OTOC approach quantifies the effective number  $K$  of environmental spins that were correlated during the preparation step [13, 43] (see SI G 3 for details).

Figure 2c compares the number  $K$  of correlated environmental spins to the qubit-probe during preparation, and the SENSIT contrast measured from the qubit-probe. Both quantities increase with the preparation time, manifesting a monotonous relation between the established OTOC measure  $K$  of non-equilibrium degree and the proposed SENSIT contrast. Measuring the OTOC involves experimental control over the environment, necessitating the ability to apply collective rotations to environmental spins and reverse the many-body evolution resulting from environmental spin-spin interaction (see SI G 3). Consequently, while OTOC measurements are feasible in e.g. NMR experiments, they are not readily available for most systems. In contrast, assessing the SENSIT contrast only requires control over the qubit-probe, specifically without the need for any control over the sensed environment.

## VI. PROBING QUANTUM INFORMATION SCRAMBLING WITH SENSIT CONTRAST

To illustrate how the SENSIT contrast, reliant on time-reversal symmetry breaking, can selectively captures information about out-of-equilibrium or quantum non-Gaussian environmental fluctuations over stationary noise fluctuations, we measure the effect of environmental scrambling

[15, 42]. In this context, we examine how the quenched state information is erased due to scrambling, consequently impacting the SENSIT contrast (Fig. 3).

Quantum information scrambling is the encoding of an initial local information into non-local degrees of freedom, in this case due to the environmental dynamics driven by the Hamiltonian of the environment  $H_E$  (Fig. 3b) [15, 42]. This in turn renders the information inaccessible by local measurements, and it is related to the autothermalization and quantum information dynamics of the environment [13, 15, 16, 42–46]. Since the qubit-probe performs a local measurement, the measurements after scrambling should match those found at equilibrium. The key control source in this context involves introducing a waiting period, denoted as the environmental scrambling time  $T_E$ , before implementing the detection of the SENSIT contrast following the quenching of the environment (Fig. 3a). In the case of a non-Gaussian environment that is stationary, the cumulant expansion terms exhibit time translation symmetry, rendering the SENSIT contrast invariant with respect to the waiting time. Conversely, an out-of-equilibrium environment relaxes towards equilibrium as a function of the waiting—scrambling—time.

The decay of the SENSIT contrast, observed in Fig. 3c, is presented as a function of the environmental scrambling time  $T_E$ . The insets provide the SDR and TSDR signals for three distinct scrambling times. The contrast between the SDR and TSDR curves diminishes as the quenched state is progressively scrambled away. These results thus effectively showcase SENSIT's ability to selectively quantify the extent to which the environment of the qubit-probe is departing from equilibrium and evolving towards equilibrium. Importantly, SENSIT enables the measurement of quantum information scrambling without relying on environmental time reversions, a requirement typical need in measurements based on OTOCs [15, 42].

## VII. SUMMARY AND OUTLOOK

While most quantum systems exhibit time reversal symmetry [38], our research unveils a fundamental breakdown of time reversal symmetry when a quantum sensor probes partial information from environments, characterized by out-of-equilibrium, non-stationary dynamics or with interactions containing quantum non-Gaussian correlations. This opens a quantum sensing paradigm, offering a lens to explore ubiquitous environments at the quantum level, where intrinsic out-of-equilibrium dynamics prevail, driven either by inherent fluctuations or quantum feedback induced by the probe [17, 18, 24, 25]. Moreover, it offers a tool for single sensors at atomic or nanoscales that can be strongly coupled with the environment, thus generating quantum non-Gaussian effects on the dephasing of the qubit-probe [25].

Our findings gain practical significance in the realm of

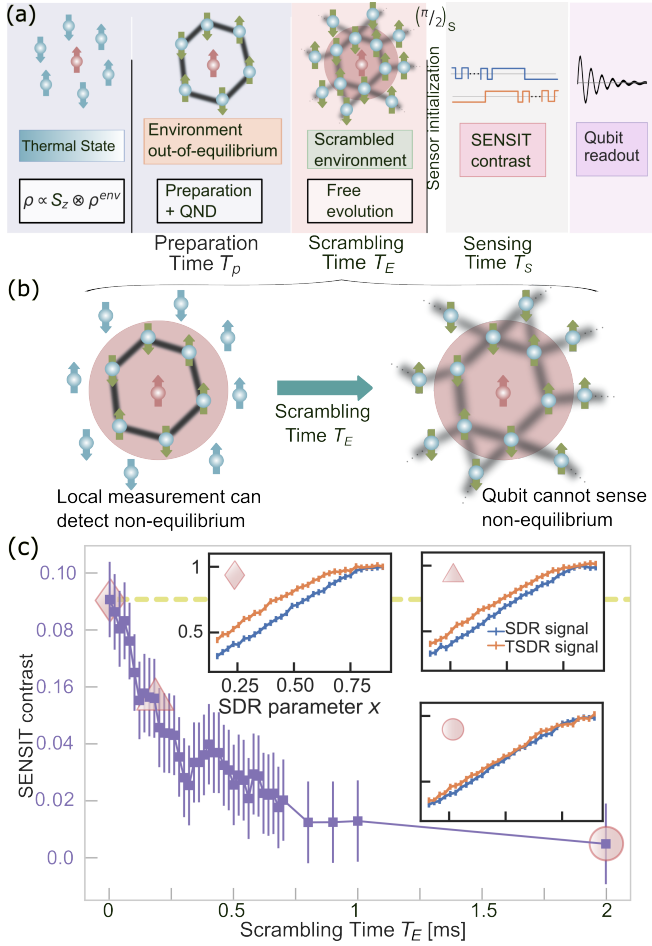


Figure 3. Sensing environmental scrambling with SENSIT. (a) Experimental protocol diagram implemented to induce nonequilibrium in the qubit environment, followed by scrambling and measurement using the SENSIT technique. (b) Schematic representation of scrambling, the process encoding localized information into non-local degrees of freedom, rendering it inaccessible by local measurements. In the limit of large environmental scrambling times  $T_E$ , the qubit’s ability to sense non-equilibrium conditions diminishes. (c) Qubit-measured SENSIT contrast as a function of the scrambling time  $T_E$ , enabling the distinction between non-stationary environmental dynamics (experimental violet curve) and non-Gaussian stationary noise (illustrative dashed yellow curve), which should remain invariant under  $T_E$ . Error bars are due to the NMR detection sensitivity. Insets display signals measured by the SDR and TSDR control sequences for different scrambling times (marked by geometrical symbols).  $N = 12$  pulses were used in our experiments. Note the separation of curves at low scrambling times converging as the quench is scrambled away.

quantum sensing. Specifically, within pump and probe schemes [47], our results open avenues for tailored measurements using qubit-probes, enabling selective detection of the environmental degrees of freedom being selectively pumped out of equilibrium. Moreover, our results holds promise for characterizing noise of time crys-

tals [48] or Floquet systems [49], specially those with partially broken time translation symmetry induced by external driving forces. This offers insights into the dynamics of such systems, providing a means to understand and quantify the intricate interplay between the quantum probe and environments with complex, time-varying characteristics [14, 24, 25].

An additional strength of our work lies in its ability to capture information scrambling of local operators, like the OTOCS, but notably without requiring environmental time reversions [15, 42]. This unique feature positions our research as a valuable tool for detecting persistent states characterized by long-lasting temporal features, such as localized modes [50]. In essence, our study not only contributes theoretical insights but also introduces practical methodologies that can be harnessed to explore and manipulate quantum systems in diverse and dynamic environments.

In conclusion, our study not only contributes fundamental insights into the breakdown of control function time reversal symmetry in quantum sensing but also presents a platform for practical applications. From tailored measurements in complex samples to probing intriguing phenomena in time crystal and Floquet systems, the potential impact of our findings offers an alternative avenue in the realm of quantum sensing technologies. This work paves the way for future research directions and applications, emphasizing the dynamic interplay between quantum sensors and complex, out-of-equilibrium environments.

## ACKNOWLEDGMENTS

This work was supported by CNEA; CONICET; ANPCyT-FONCyT PICT-2017-3156, PICT-2017-3699, PICT-2018-4333, PICT-2021-GRF-TI-00134, PICT-2021-I-A-00070; PIP-CONICET (11220170100486CO); UNCuyo SIIP Tipo I 2019-C028, 2022-C002, 2022-C030; Instituto Balseiro; Collaboration programs between the MINCyT (Argentina) and, MAECI (Italy) and MOST (Israel).

## Appendix A: Cumulant expansion for the qubit-probe signal decay

In this section we derive the cumulant expansion of the decoherence factor  $\mathcal{J}$  given by Eq. (2) in the main text. Initially, we describe the signal decay of a controlled qubit-probe that dephases due to the influence of an arbitrary quantum environment. We then express it as a function of the correlation functions of the environmental fluctuation, subsequently deriving the cumulant expansion representation.

### 1. Qubit-probe dephasing in terms of the environmental correlation functions

We denote the initial state of the full system as  $\rho(t=0) = \rho_0$  and we assume it is separable

$$\rho_0 = pS_x \otimes \rho_E, \quad (\text{A.1})$$

where  $p$  is the polarization of the qubit and the qubit-probe state  $S_x$  is in the  $x$  direction. Notice that, we do not explicitly write terms proportional to the qubit identity  $\mathbb{I}_S$  in the density matrix, as they do not contribute to the qubit-probe signal. We calculate the decay of in-plane polarization  $M = \frac{2}{p} \langle S_+ \otimes \mathbb{I}_E U(T_s) \rho_0 U^\dagger(T_s) \rangle$  of the qubit sensor after dephasing

$$M = \frac{2}{p} \langle S_+ \otimes \mathbb{I}_E U(T_s) \rho_0 U^\dagger(T_s) \rangle = \frac{2}{p} \langle S_+ \otimes \mathbb{I}_E U(T_s) pS_x \otimes \rho_E U^\dagger(T_s) \rangle \quad (\text{A.2})$$

where  $\mathbb{I}_E$  is the environmental identity matrix and  $U(T_s)$  is the evolution operator. As described in the maintext,  $U(T_s) = \mathcal{T} e^{-i \int_0^{T_s} dt f(t) S_z B(t)}$ , and evaluating the trace over the qubit-degrees of freedom in Eq. (A.2), we find

$$\begin{aligned} M &= \left\langle \left( \mathcal{T} e^{\frac{i}{2} \int_0^{T_s} dt f(t) B(t)} \right) \rho_E \left( \mathcal{T} e^{-\frac{i}{2} \int_0^{T_s} dt f(t) B(t)} \right)^\dagger \right\rangle \\ &= \left\langle \left( \mathcal{T} e^{\frac{i}{2} \int_0^{T_s} dt f(t) B(t)} \right) \rho_E \left( \tilde{\mathcal{T}} e^{\frac{i}{2} \int_0^{T_s} dt f(t) B(t)} \right) \right\rangle, \end{aligned} \quad (\text{A.3})$$

where  $\tilde{\mathcal{T}}$  is the anti-time-order superoperator. Considering  $M$  as a functional of  $f$ , we can perform a functional Taylor expansion in  $f$  to obtain

$$M = \sum_n \frac{1}{n!} \int dt_1 \cdots \int dt_n f(t_1) \cdots f(t_n) \left[ \frac{\delta}{\delta f(t_1)} \cdots \frac{\delta}{\delta f(t_n)} M \right] \Big|_{f=0}, \quad (\text{A.4})$$

where  $\frac{\delta}{\delta f(t)}$  represents functional differentiation with respect to  $f(t)$ . Defining the environmental correlation functions as

$$G_n(t_1, \dots, t_n) = (-i)^n \left[ \frac{\delta}{\delta f(t_1)} \cdots \frac{\delta}{\delta f(t_n)} M \right] \Big|_{f=0} \quad (\text{A.5})$$

$$= (-i)^n \left[ \frac{\delta}{\delta f(t_1)} \cdots \frac{\delta}{\delta f(t_n)} \left\langle \left( \mathcal{T} e^{\frac{i}{2} \int_0^{T_s} dt f(t) B(t)} \right) \rho_E \left( \mathcal{T} e^{-\frac{i}{2} \int_0^{T_s} dt f(t) B(t)} \right)^\dagger \right\rangle \right] \Big|_{f=0}, \quad (\text{A.6})$$

we find that

$$M = \sum_n \frac{i^n}{n!} \int_0^{T_s} dt_1 \cdots \int dt_n f(t_1) \cdots f(t_n) G_n(t_1, \dots, t_n). \quad (\text{A.7})$$

Notice that the correlation functions  $G_n(t_1, \dots, t_n)$  are symmetric under exchange of their arguments, i.e.  $G_n(t_1, \dots, t_i, \dots, t_j, \dots, t_n) = G_n(t_1, \dots, t_j, \dots, t_i, \dots, t_n)$ . They depend solely on the environmental time-dependent noise operator  $B(t)$  and initial state  $\rho_E$  as

$$G_n(t_1, \dots, t_n) = \frac{1}{2^{n-1}} \langle \{B(t_1), \{B(t_2), \{\dots, B(t_n)\} \dots\} \} \rho_E \rangle, \quad (\text{A.8})$$



for  $t_1 \leq t_2 \leq \dots \leq t_n$ . These correlation functions are the mean value of the nested anti-commutators  $\{\cdot, \cdot\}$  of the noise operator in the environmental state  $\rho_E$ . The lowest order ones are

$$\begin{aligned} G_0 &= 1, \\ G_1(t_1) &= \langle B(t_1) \rho_E \rangle, \\ G_2(t_1, t_2) &= \frac{1}{2} \langle \{B(t_1), B(t_2)\} \rho_E \rangle, \\ G_3(t_1, t_2, t_3) &= \frac{1}{4} \langle \{B(t_1), \{B(t_2), B(t_3)\}\} \rho_E \rangle, \end{aligned}$$

for  $t_1 \leq t_2 \leq t_3$ . While this procedure is perturbative, the knowledge of the correlation functions completely determines the decay of the qubit even in the non-perturbative regime.

## 2. The cumulant expansion for the qubit-signal decay

The correlation functions  $G_n$  completely describe the decay of the qubit-probe. However, certain effects can be more easily described using the cumulants, e.g. non-Gaussianity, separability of the effects of independent processes, exponential signal decay and quantification of the control time-reversal symmetry breaking. Expanding in a perturbation series the decoherence factor  $\mathcal{J}$  with  $M = e^{-\mathcal{J}}$ , we obtain Eq. (2) of the main text

$$\mathcal{J} = - \sum_n \frac{i^n}{n!} \int_0^{T_s} dt_1 \dots \int_0^{T_s} dt_n f(t_1) \dots f(t_n) W_n(t_1, \dots, t_n), \quad (\text{A.9})$$

where  $W_n$  are the cumulants of the environmental correlation functions. Then by expanding  $M = \sum_n \frac{(-1)^n}{n!} \mathcal{J}^n$ , we find the connection between the cumulants  $W_n$  and the correlation functions  $G_n$

$$\begin{aligned} W_0 &= 0 \\ W_1(t_1) &= G_1(t_1) \\ W_2(t_1, t_2) &= G_2(t_1, t_2) - W_1(t_1)W_1(t_2) \\ W_3(t_1, t_2, t_3) &= G_3(t_1, t_2, t_3) - W_2(t_1, t_2)W_1(t_3) - W_1(t_1)W_2(t_2, t_3) - W_1(t_2)W_2(t_3, t_1) - W_1(t_1)W_1(t_2)W_1(t_3). \end{aligned}$$

The general guideline for constructing the  $n$ -th order cumulant  $W_n$ , involves subtracting from  $G_n$  all possible combinations of functions generated by taking products of cumulants with orders less than  $n$  [51]. Specifically, for a Gaussian environment, Wick's theorem dictates that  $W_n = 0$  for  $n > 2$  [51].

Since the correlation functions  $G_n$  are real, the cumulants  $W_n$  are also real. Therefore the cumulants of odd order contribute to the qubit signal phase  $\arg M = -\text{Im}(\mathcal{J})$  based on Eq. (A.9)

$$\text{Im}(\mathcal{J}) = - \sum_n \frac{(-1)^n}{(2n+1)!} \int_0^{T_s} dt_1 \dots \int_0^{T_s} dt_{2n+1} f(t_1) \dots f(t_{2n+1}) W_{2n+1}(t_1, \dots, t_{2n+1}), \quad (\text{A.10})$$

and the cumulants of even order to the absolute value of the qubit-signal  $|M| = e^{-\text{Re}(\mathcal{J})}$ , with

$$\text{Re}(\mathcal{J}) = - \sum_n \frac{(-1)^n}{(2n)!} \int_0^{T_s} dt_1 \dots \int_0^{T_s} dt_{2n} f(t_1) \dots f(t_{2n}) W_{2n}(t_1, \dots, t_{2n}). \quad (\text{A.11})$$

## Appendix B: SENSIT Contrast

We here calculate the SENSIT contrast based on the comparison between the qubit-probe signal  $M_f$ , when the control modulating function is  $f(t)$ , with the signal  $M_{f_T}$ , for the time reversed control  $f_T(t) = f(T_s - t)$ . The corresponding decoherence factors based on Eq. (A.9) are

$$\begin{aligned} \mathcal{J}_f &= - \sum_n \frac{i^n}{n!} \int_0^{T_s} dt_1 \dots \int_0^{T_s} dt_n f(t_1) \dots f(t_n) W_n(t_1, \dots, t_n), \\ \mathcal{J}_{f_T} &= - \sum_n \frac{i^n}{n!} \int_0^{T_s} dt_1 \dots \int_0^{T_s} dt_n f_T(t_1) \dots f_T(t_n) W_n(t_1, \dots, t_n), \end{aligned}$$

respectively. Changing variables we can rewrite the last equation as  $\mathcal{J}_{f_T} = -\sum_n \frac{(-i)^n}{n!} \int_0^{T_s} dt_1 \cdots \int_0^{T_s} dt_n f(t_1) \cdots f(t_n) W_n(T_s - t_1, \dots, T_s - t_n)$ .

Then the difference between the attenuation factors is  $\Delta\mathcal{J} = \mathcal{J}_f - \mathcal{J}_{f_T}^{(*)}$ , where  $(*)$  is complex conjugation applied only for magnetic-type cases. The distinction between electric- and magnetic-type cases is described in SI C. In terms of the cumulant differences, we obtain

$$\Delta\mathcal{J} = -\sum_n \frac{i^n}{(n)!} \int_0^{T_s} dt_1 \cdots \int_0^{T_s} dt_n f(t_1) \cdots f(t_n) \Delta W_n(t_1, \dots, t_n), \quad (\text{A.12})$$

where the cumulant differences are

$$\Delta W_n(t_1, \dots, t_n) = W_n(t_1, \dots, t_n) - (\pm 1)^n W_n(T_s - t_1, \dots, T_s - t_n),$$

with  $\pm 1$  being 1 for electric- and  $-1$  for magnetic-type cases. For cumulants of even order, this distinction is irrelevant as  $(\pm 1)^{2n} = 1$ , leading to Eq. (6) in the main text.

As stated in the main text, they measure the degree of time reversal symmetry breaking of the control operations of the qubit-probe, acting as a kind of order parameters. As shown in SI A2,  $(-i)^n W_n$  is real for  $n$  and imaginary for  $n$  odd. Consequently,  $\Delta\mathcal{J}$  separates into real and imaginary components. The real (resp. imaginary) component is influenced only by cumulants of even (resp. odd) order, corresponding to a difference in the magnitude (resp. phase) of the qubit-probe signals  $M_f$  and  $M_{f_T}$ . Explicitly real component

$$\text{Re}\Delta\mathcal{J} = \ln \left| \frac{M_{f_T}}{M_f^{(*)}} \right| = \ln \left| \frac{M_{f_T}}{M_f} \right| = -\sum_n \frac{(-1)^n}{(2n)!} \int_0^{T_s} dt_1 \cdots \int_0^{T_s} dt_{2n} f(t_1) \cdots f(t_{2n}) \Delta W_{2n}(t_1, \dots, t_{2n})$$

corresponds to a difference in the magnitude of the qubit-probe signals, and it is defined by cumulant differences of even order  $\Delta W_{2n}$ . This thus demonstrates Eq. (5) of the main text. Analogously, the imaginary component

$$\text{Im}\Delta\mathcal{J} = \arg \left( \frac{M_{f_T}}{M_f^{(*)}} \right) = -\sum_{n=0}^{\infty} \frac{(-1)^n}{(2n+1)!} \int_0^{T_s} dt_1 f(t_1) \cdots \int_0^{T_s} dt_{2n+1} f(t_{2n+1}) \Delta W_{2n+1}(t_1, \dots, t_{2n+1})$$

corresponds to a difference in the phases of the qubit signals, and it is defined by the cumulant differences of odd order  $\Delta W_{2n+1}$ .

### Appendix C: Conditions in the environment for attaining time-reversal symmetry of the qubit-probe control

In this Section, we analyze the conditions required on the environment to satisfy the time-reversal symmetry of the control on the qubit-probe. Based on the expression for the SENSIT contrast of Eq. (A.12) and Eq. (5) of the maintext, the cumulant difference  $\Delta W_n(t_1, \dots, t_{2n}) = 0$  should vanish.

To obtain  $\Delta W_n(t_1, \dots, t_n) = 0$  for all sensing times  $T_s$ , it is required for the cumulant functions to have time translation symmetry and that  $W_n(t_1, \dots, t_{2n}) = (\pm 1)^n W_n(-t_1, \dots, -t_{2n})$ , where the sign  $(\pm 1)^n$  depends on the nature of the noise operator and will be explained later in this section. The first condition is attained if the environmental noise operator fluctuations are stationary. The second one if they have time-reversal symmetry. In Sec. C1 we thus evaluate the effects of the time translation symmetry of stationary environments and in Sec. C2 we determine the effects of time-reversal symmetry in the environment.

#### 1. Time translation symmetry of the correlation functions and cumulants: a stationary environment

To obtain  $\Delta W_n(t_1, \dots, t_n) = 0$ , we need the cumulants to have time translation symmetry

$$W_n(t_1 + \Delta t, \dots, t_n + \Delta t) = W_n(t_1, \dots, t_n).$$

As the cumulants are written in terms of the environment correlation functions  $G_n$  of Eq. (A.8), we thus need them to have time translation symmetry  $G_n(t_1 + \Delta t, \dots, t_n + \Delta t) = G_n(t_1, \dots, t_n)$ . As the noise operators are defined by

$B(t) = e^{itH_E} B e^{-itH_E}$ , where  $H_E$  is the environment Hamiltonian, we obtain

$$\begin{aligned}
G_n(t_1 + \Delta t, \dots, t_n + \Delta t) &= \frac{1}{2^{n-1}} \langle \{B(t_1 + \Delta t), \{B(t_2 + \Delta t), \{\dots, B(t_n + \Delta t)\} \dots\} \} \rho_E \rangle \\
&= \frac{1}{2^{n-1}} \langle \{e^{i\Delta t H_E} B(t_1) e^{-i\Delta t H_E}, \{e^{i\Delta t H_E} B(t_2) e^{-i\Delta t H_E}, \{\dots, e^{i\Delta t H_E} B(t_n) e^{-i\Delta t H_E}\} \dots\} \} \rho_E \rangle \\
&= \frac{1}{2^{n-1}} \langle e^{i\Delta t H_E} \{B(t_1), \{B(t_2), \{\dots, B(t_n)\} \dots\} \} e^{-i\Delta t H_E} \rho_E \rangle \\
&= \frac{1}{2^{n-1}} \langle \{B(t_1), \{B(t_2), \{\dots, B(t_n)\} \dots\} \} e^{-i\Delta t H_E} \rho_E e^{i\Delta t H_E} \rangle.
\end{aligned}$$

Therefore we need the environment to be in a stationary state such that  $e^{-i\Delta t H_E} \rho_E e^{i\Delta t H_E} = \rho_E$  for all translation times  $\Delta t$ . Then

$$\begin{aligned}
G_n(t_1 + \Delta t, \dots, t_n + \Delta t) &= \frac{1}{2^{n-1}} \langle \{B(t_1), \{B(t_2), \{\dots, B(t_n)\} \dots\} \} e^{-i\Delta t H_E} \rho_E e^{i\Delta t H_E} \rangle \\
&= \frac{1}{2^{n-1}} \langle \{B(t_1), \{B(t_2), \{\dots, B(t_n)\} \dots\} \} \rho_E \rangle \\
&= G_n(t_1, \dots, t_n).
\end{aligned}$$

The cumulants thus have time translation symmetry if and only if the environment is in a stationary state.

## 2. Time reversal symmetry of the correlation functions and cumulants of the environment

To satisfy the second condition  $W_n(t_1, \dots, t_{2n}) = (\pm 1)^n W_n(-t_1, \dots, -t_{2n})$ , we need the cumulants to have time-reversal symmetry. We thus require our full system with time-reversal symmetry. Time reversal symmetry in simple terms involves reversing the direction of time in the equations that describe the evolution of a system. If these equations remain unchanged when time is reversed, the system is said to exhibit time reversal symmetry. Quantum mechanics is unitary, i.e. the evolution operator  $U(t)$  is unitary and thus invertible  $U^\dagger(t) = U^{-1}(t)$ . When a quantum system has time-reversal symmetry, this can be expressed with the time reversal operator  $T$ , an anti-unitary operator that commutes with the system Hamiltonian  $[T, H] = 0$  and such that  $T^{-1}U(t)T = U^{-1}(t)$  [38].

In our particular case, to have time-reversal symmetry there exists some anti-unitary operator  $T = T_S \otimes T_E$  such that the full Hamiltonian  $H$  is  $T$ -invariant, i.e.  $T^{-1}HT = H$ . This implies in particular that  $T_S^{-1}S_zT_S = \pm S_z$ , and  $T_E^{-1}BT_E = \pm B$ , as the qubit-environment interaction  $\propto S_z B$  must be  $T$ -invariant. We call the cases when  $B$  commutes with the time reversal operator  $[B, T_{\text{env}}] = 0$  of the electric-type, as it is the case when  $B$  represents gate charges, voltages, electric fields, polarizations, etc. Analogously, we call the case when  $B$  anticommutes with the time reversal operator  $\{B, T_{\text{env}}\} = 0$  of the magnetic-type, as it is the case when  $B$  represents currents, magnetic fields, magnetizations, etc. In our experimental realization the noise operator is a magnetic field, therefore we performed experiments in a magnetic-type case.

The time reversal operator  $T_E$  must satisfy  $T_E^2 = \pm 1$  [38], therefore  $T_E^{-1} = \pm T_E$ . This in turn implies

$$\begin{aligned}
T_E^{-1}U_E(t)T_E &= U_E^\dagger(t), \\
T_E^{-1}U_E^\dagger(t)T_E &= U_E(t), \\
T_E U_E(t)T_E^{-1} &= U_E^\dagger(t), \\
T_E U_E^\dagger(t)T_E^{-1} &= U_E(t),
\end{aligned}$$

where  $U_E(t) = e^{-iH_E t}$  is the environmental evolution operator. This thus implies that  $T_E^{-1}B(t)T_E = T_E^{-1}U_E^\dagger(t)BU_E(t)T_E = \pm B(-t)$ .

Based on this properties of the time-reversal operator, we analyze the behavior of the cumulants under the time-reversal. As the cumulants are written in terms of the environment correlation functions  $G_n$  of Eq. (A.8), for the cumulants to have time-reversal symmetry it is necessary and sufficient for the correlation functions to have time reversal symmetry  $G_n(t_1, \dots, t_n) = (\pm 1)^n G_n(-t_1, \dots, -t_n)$ . Without loss of generality we consider  $t_1 \leq t_2 \leq \dots \leq t_n$ , and thus  $-t_n \leq -t_{n-1} \leq \dots \leq -t_1$ . Therefore

$$G_n(-t_1, \dots, -t_n) = \frac{(\pm 1)^n}{2^{n-1}} \langle \{B(-t_n), \{B(-t_{n-1}), \{\dots, B(-t_1)\} \dots\} \} \rho_E \rangle.$$

We can now achieve to this expression using  $T_E$  as

$$G_n(-t_1, \dots, -t_n) = \frac{(\pm 1)^n}{2^{n-1}} \langle \{T_E^{-1} B(t_n) T_E, \{T_E^{-1} B(t_{n-1}) T_E, \{\dots, T_E^{-1} B(t_1) T_E\} \dots\} \} \rho_E \rangle .$$

The product of the operators  $T_E$  and  $T_E^{-1}$  is the identity and we get

$$G_n(-t_1, \dots, -t_n) = \frac{(\pm 1)^n}{2^{n-1}} \langle \{B(t_n), \{B(t_{n-1}), \{\dots, B(t_1)\} \dots\} \} T_E \rho_E T_E^{-1} \rangle .$$

We thus obtain that for the cumulants to have time-reversal symmetry, we need the environmental state  $\rho_E$  to be  $T_E$ -invariant, i.e.  $T_E \rho_E T_E^{-1} = \rho_E$ . If we assume this, we obtain

$$G_n(-t_1, \dots, -t_n) = \frac{(\pm 1)^n}{2^{n-1}} \langle \{B(t_n), \{B(t_{n-1}), \{\dots, B(t_1)\} \dots\} \} \rho_E \rangle . \quad (\text{A.13})$$

This differs from  $(\pm 1)^n G_n(t_1, \dots, t_n)$  in the ordering of the noise operators in the anticommutators. For  $G_1$  and  $G_2$ , Eq. (A.13) becomes  $G_1(t_1) = \pm G_1(-t_1)$  and  $G_2(t_1, t_2) = G_2(-t_1, -t_2)$ . However from  $n = 3$  and forth,  $G_n(t_1, \dots, t_n)$  differs from  $(\pm 1)^n G_n(-t_1, \dots, -t_n)$ .

For example for  $t_1 \leq t_2 \leq t_3$ ,

$$\begin{aligned} G_3(t_1, t_2, t_3) &= \frac{1}{4} \langle \{B(t_1), \{B(t_2), B(t_3)\} \} \rho_E \rangle \\ &= \frac{1}{4} \langle [B(t_1)B(t_2)B(t_3) + B(t_1)B(t_3)B(t_2) + B(t_2)B(t_3)B(t_1) + B(t_3)B(t_2)B(t_1)] \rho_E \rangle , \end{aligned}$$

and

$$\begin{aligned} \pm G_n(-t_1, -t_2, -t_3) &= \frac{1}{4} \langle \{B(t_3), \{B(t_2), B(t_1)\} \} \rho_E \rangle \\ &= \frac{1}{4} \langle [B(t_3)B(t_2)B(t_1) + B(t_3)B(t_1)B(t_2) + B(t_2)B(t_1)B(t_3) + B(t_1)B(t_2)B(t_3)] \rho_E \rangle . \end{aligned}$$

Therefore

$$\begin{aligned} G_3(t_1, t_2, t_3) \mp G_n(-t_1, -t_2, -t_3) &= \\ &= \frac{1}{4} \langle [B(t_1)B(t_3)B(t_2) + B(t_2)B(t_3)B(t_1) - B(t_3)B(t_1)B(t_2) - B(t_2)B(t_1)B(t_3)] \rho_E \rangle \\ &= \frac{1}{4} \langle \{[B(t_1)B(t_3) - B(t_3)B(t_1)] B(t_2) + B(t_2) [B(t_3)B(t_1) - B(t_1)B(t_3)] \} \rho_E \rangle \\ &= \frac{1}{4} \langle \{[B(t_1), B(t_3)] B(t_2) + B(t_2) [B(t_3), B(t_1)] \} \rho_E \rangle \\ &= \frac{1}{4} \langle [[B(t_1), B(t_3)], B(t_2)] \rho_E \rangle . \end{aligned}$$

This thus shows an example on how the time reversal symmetry of higher order correlation functions is broken and the breaking is proportional to commutators of the noise operator at different times.

Nevertheless, if the environment is classical or it is at the high temperature limit, one can make a semiclassical approximation of the noise operators and replace

$$\{B(t_1), B(t_2)\} \sim 2B(t_1)B(t_2) \sim 2B(t_2)B(t_1) .$$

In these cases, the correlation functions become

$$G_n(t_1, \dots, t_n) = \langle B(t_1)B(t_2) \dots B(t_n) \rho_E \rangle = (\pm 1)^n G_n(-t_1, \dots, -t_n),$$

and therefore also the cumulants satisfy

$$W_n(t_1, \dots, t_n) = (\pm 1)^n W_n(-t_1, \dots, -t_n),$$

thus satisfying the time-reversal symmetry in the cumulants.

When the environment is Gaussian, either quantum or classical, the only non-zero cumulants are  $W_1$  and  $W_2$ . Since  $G_1(t_1) = \pm G_1(-t_1)$  and  $G_2(t_1, t_2) = G_2(-t_1, -t_2)$ , then  $W_1(t_1) = \pm W_1(-t_1)$  and  $W_2(t_1, t_2) = W_2(-t_1, -t_2)$ . Analogously, when the qubit is weakly coupled to its environment, then the phase is dominated by  $W_1$  and the decay by  $W_2$ , and the environment can be well approximated as a Gaussian environment even if it is a quantum environment.



The cumulants thus only have time-reversal symmetry when the contributions of noise operators commute at different times, if the environment is quantum and non-Gaussian in the sense that is described with cumulants of order higher than 2.

Summarizing, the results presented here mean that the time-reversal symmetry is only attained when all the relevant cumulants to the qubit-probe dephasing satisfy

$$W_n(t_1, \dots, t_n) = (\pm 1)^n W_n(-t_1, \dots, -t_n). \quad (\text{A.14})$$

Instead, the time-reversal symmetry is broken when the environment is quantum, at low temperature, non-Gaussian, and strongly coupled to the qubit.

### 3. Time reversal symmetry of the decoherence factor

When the environment is in a stationary state, and satisfies Eq. (A.14), this means that

$$\mathcal{J}_{f_T} = - \sum_n (\pm 1)^n \frac{i^n}{n!} \int_0^{T_s} dt_1 \cdots \int_0^{T_s} dt_n f(t_1) \cdots f(t_n) W_n(t_1, \dots, t_n),$$

or, equivalently,

$$\begin{aligned} \text{Re}(\mathcal{J}_{f_T}) &= \text{Re}(\mathcal{J}_{f_T}) , \\ \text{Im}(\mathcal{J}_{f_T}) &= \pm \text{Im}(\mathcal{J}_{f_T}) , \end{aligned}$$

where  $\pm = +$  for electric-type noise and  $\pm = -$  for magnetic-type noise. This means that for electric-type noise  $M_{f_T} = M_f$ , and for magnetic noise  $M_{f_T} = M_f^*$ .

### Appendix D: Filter out of stationary environmental noise sources by the SENSIT contrast

We here demonstrate the selective property of the SENSIT contrast to filter in environmental sources that leads to the breaking of the time reversed symmetry of the qubit-control, i.e. nonstationary or quantum non-Gaussian noise sources. The SENSIT control filters out the noise sources that induce decoherence on the qubit-probe, but do not induce a breaking in the control time-reversal symmetry. Formally, we consider an environment containing two separated subsystems  $a$  and  $b$ , such that  $a$  is either out of equilibrium inducing non-stationary noise sources or it is quantum non-Gaussian and  $b$  is an environment that is stationary and effectively Gaussian or classical. This means both  $a$  and  $b$  induce decoherence on the qubit-probe, but only  $a$  induces time-reversal symmetry breaking on the control. We write the environment Hilbert space as  $\mathcal{H}_E = \mathcal{H}_a \otimes \mathcal{H}_b$ , the noise operator  $B = B_a \otimes \mathbb{I}_b + \mathbb{I}_a \otimes B_b$ , the environmental Hamiltonian  $H_E = H_a \otimes \mathbb{I}_b + \mathbb{I}_a \otimes H_b$  and the initial environmental state as  $\rho_E = \rho_a \otimes \rho_b$ . The environments have thus an independent initial state, evolve independently and each of them adds a separated noise contribution to the qubit-probe. For example, in the experiments we carried out on this work, the environment  $a$  would be the spin network of  $^1\text{H}$  nuclei, while  $b$  would be any other sources of decoherence, e.g. the electrons and phonons of the sample, cosmic rays and radiation going through it, the current fluctuations in the magnet, the noise induced by electrical installations, etc. Since the environmental subsystems do not interact with each other, the evolution of the noise operator with respect to the environmental Hamiltonian is  $B(t) = B_a(t) \otimes \mathbb{I}_b + \mathbb{I}_a \otimes B_b(t)$ , where  $B_i(t) = e^{iH_i t} B_i e^{-iH_i t}$  for  $i = a, b$ . The evolution operator  $\mathcal{T} e^{\frac{i}{2} \int_0^{T_s} dt f(t) B(t)}$  in Eq. (A.3) is also separable

$$\mathcal{T} e^{\frac{i}{2} \int_0^{T_s} dt f(t) B(t)} = \mathcal{T} e^{\frac{i}{2} \int_0^{T_s} dt f(t) B_a(t)} \otimes \mathcal{T} e^{\frac{i}{2} \int_0^{T_s} dt f(t) B_b(t)}.$$

The decay of the qubit magnetization thus becomes

$$M = \left\langle \left( \mathcal{T} e^{\frac{i}{2} \int_0^{T_s} dt f(t) B_a(t)} \right) \rho_a \left( \mathcal{T} e^{-\frac{i}{2} \int_0^{T_s} dt f(t) B_a(t)} \right)^\dagger \right\rangle \times \left\langle \left( \mathcal{T} e^{\frac{i}{2} \int_0^{T_s} dt f(t) B_b(t)} \right) \rho_b \left( \mathcal{T} e^{-\frac{i}{2} \int_0^{T_s} dt f(t) B_b(t)} \right)^\dagger \right\rangle.$$

We now define the cumulants  $W_n^{a/b}$  of the subsystems as the cumulants of the respective noise operators  $B^{a/b}(t)$ . We can thus write the contributions to the decay in terms of

$$\left\langle \left( \mathcal{T} e^{\frac{i}{2} \int_0^{T_s} dt f(t) B_i(t)} \right) \rho_i \left( \mathcal{T} e^{-\frac{i}{2} \int_0^{T_s} dt f(t) B_i(t)} \right)^\dagger \right\rangle = \exp \left[ \sum_n \frac{(i)^n}{n!} \int_0^{T_s} dt_1 \cdots \int_0^{T_s} dt_n f(t_1) \cdots f(t_n) W_n^i(t_1, \dots, t_n) \right],$$

and we obtain the decoherence factor as

$$\mathcal{J} = - \sum_n \frac{(i)^n}{n!} \int_0^{T_s} dt_1 \cdots \int_0^{T_s} dt_n f(t_1) \cdots f(t_n) [W_n^a(t_1, \dots, t_n) + W_n^b(t_1, \dots, t_n)] ,$$

and compare with Eq. (A.9), we obtain that the cumulants of the environment  $W_n = W_n^a + W_n^b$  are the sum of the cumulants of each subsystem. Since the environment  $b$  is neither non-stationary nor quantum non-Gaussian, the cumulants  $W_n^b$  are symmetric under time reversed control. Therefore, the SENSIT contrast is

$$\Delta \mathcal{J} = - \sum_n \frac{i^n}{(n)!} \int_0^{T_s} dt_1 \cdots \int_0^{T_s} dt_n f(t_1) \cdots f(t_n) \Delta W_n^a(t_1, \dots, t_n) ,$$

where  $\Delta W_n^a(t_1, \dots, t_{2n}) = W_n^a(t_1, \dots, t_{2n}) - W_n^a(T_s - t_1, \dots, T_s - t_{2n})$ . This thus shows how the SENSIT contrast is independent of all properties of  $b$ , and is in fact the same as what would be obtained if  $a$  were the entire environment of the qubit-probe. This shows that SENSIT is filtering out all noise sources leading to time-reversal symmetry on the qubit control, while maintaining sensitivity to those out of equilibrium or quantum non-Gaussian.

### Appendix E: SENSIT contrast with an environment near to a stationary state

To give an example on how the distance to equilibrium is encoded in the SENSIT contrast, we consider a simple but general case where the environment is near to a stationary state  $\rho_E^{(0)}$ . We consider that quantum non-Gaussian contributions to the cumulants are negligible. That is,  $\rho_E^{(0)}$  is a state where the cumulants have time reversal symmetry in the qubit-probe control  $\Delta W_n = 0$ . We consider the environmental state to be  $\rho_E = \rho_E^{(0)} + \epsilon \rho_E^{(1)}$ , where  $\rho_E^{(1)}$  is a constant perturbation to the environmental state with  $\epsilon$  quantifying the distance to equilibrium. Under these conditions, the cumulants can be expanded in the distance  $\epsilon$  as  $W_n = W_n^{(0)} + \epsilon W_n^{(1)} + \mathcal{O}(\epsilon^2)$ , where  $W_n^{(0)}$  is the  $n$ -th cumulant for the environmental state  $\rho_E^{(0)}$ , and  $W_n^{(1)}$  depends on both environmental contributions  $\rho_E^{(0)}$  and  $\rho_E^{(1)}$ . For example, for  $n = 2$

$$W_2^{(1)}(t_1, t_2) = \langle \{B(t_1), B(t_2)\} \rho_E^{(1)} \rangle - \langle B(t_1) \rho_E^{(1)} \rangle \langle B(t_2) \rho_E^{(0)} \rangle - \langle B(t_1) \rho_E^{(0)} \rangle \langle B(t_2) \rho_E^{(1)} \rangle .$$

Since we consider that  $\rho_E^{(0)}$  has time reversal symmetry in the qubit-probe control, the main contributions to  $\Delta W_n$  will be linear in  $\epsilon$  and due to the term

$$\Delta W_n^{(1)}(t_1, \dots, t_n) = W_n^{(1)}(t_1, \dots, t_n) - (\pm 1)^n W_n^{(1)}(T_s - t_1, \dots, T_s - t_n) .$$

The measured SENSIT contrast is thus

$$\Delta \mathcal{J} = -\epsilon \sum_n \frac{i^n}{(n)!} \int_0^{T_s} dt_1 \cdots \int_0^{T_s} dt_n f(t_1) \cdots f(t_n) \Delta W_n^{(1)}(t_1, \dots, t_n) + \mathcal{O}(\epsilon^2) ,$$

manifesting that when the environment is near to a state that satisfies the conditions for time-reversal symmetry in the qubit-probe control, the SENSIT contrast is proportional to the parameter  $\epsilon$  that quantifies the distance to the stationary environmental state.

### Appendix F: SENSIT Contrast of a Quenched Ornstein-Uhlenbeck Process

We consider the paradigmatic example of a quenched OU process for the noise operator fluctuations, with a self-correlation time  $\tau$  and the standard deviation  $\sigma_0$  at equilibrium, i.e. at long times. This stochastic process is Gaussian with zero mean, thus all cumulants with  $n \neq 2$  are null  $W_n = 0$ . The quench is generated by an out-of-equilibrium initial condition, corresponding to a Gaussian distribution with a standard deviation different from the one at equilibrium  $\sigma \neq \sigma_0$ . The self-correlation function of the quenched process is

$$W_2(t_1, t_2) = W_2^{\text{Eq}}(t_1, t_2) + W_2^{\text{Q}}(t_1, t_2) ,$$

where

$$W_2^{\text{Eq}}(t_1, t_2) = \sigma_0 e^{-\frac{|t_1 - t_2|}{\tau}}$$

and

$$W_2^{\text{Q}}(t_1, t_2) = (\sigma - \sigma_0) e^{-\frac{t_1 + t_2}{\tau}}$$

are the equilibrium and quench contributions to the correlation function [18]. The SENSIT contrast measured from a qubit-probe coupled to this noise process is  $\text{Re}\Delta\mathcal{J} = -\int_0^{T_s} dt_1 f(t_1) \int_0^{T_s} dt_2 f(t_2) \left[ W_2^Q(t_1, t_2) - W_2^Q(T_s - t_1, T_s - t_2) \right]$ . Since  $W_2^{\text{Eq}}(t_1, t_2) = W_2^{\text{Eq}}(T_s - t_1, T_s - t_2)$ , the equilibrium correlation function does not contribute to the SENSIT contrast. After replacing the cumulants, the SENSIT contrast can be written as  $\text{Re}\Delta\mathcal{J} = (\sigma - \sigma_0) \Sigma[f]$ , with

$$\Sigma[f] = -\frac{1}{2} \left[ \left( \int_0^{T_s} dt f(t) e^{-\frac{t}{\tau}} \right)^2 - \left( \int_0^{T_s} dt f(t) e^{-\frac{T_s-t}{\tau}} \right)^2 \right].$$

Note that the SENSIT contrast is proportional to  $(\sigma - \sigma_0)$ , i.e. a variance distance defining how far from equilibrium the initial state of the environment is, weighted by the term  $\Sigma[f]$  that measures the ability of the chosen control modulation function  $f$  to detect the time-reversal symmetry breaking. This thus sets a paradigmatic example about how the SENSIT contrast is proportional to  $(\sigma - \sigma_0)$  quantifying the distance from the initial state of the environment to its stationary state at equilibrium.

## Appendix G: Solid-state NMR Quantum Simulations

### 1. Experimental setup and system

The quantum simulations were performed with solid-state NMR experiments on a Bruker Avance III HD 9.4T WB spectrometer with a  $^1\text{H}$  resonance frequency of 400.15 MHz and a  $^{13}\text{C}$  resonance frequency of 100.61 MHz. We used the nuclear spins of a polycrystalline adamantane  $\text{C}_{10}\text{H}_{16}$  sample to set up the qubit-probe and its environment. Most hydrogen nuclei (98.93%) in the sample are protons, with a spin  $1/2$ , while only approximately 1.07% of the carbons are  $^{13}\text{C}$ , with spin  $1/2$ , the remaining carbons has no magnetic moment. The low concentration of  $^{13}\text{C}$  allows to neglect the interaction between them as the interaction with the hydrogens is dominant. We therefore consider the sample as an ensemble of  $^{13}\text{C}$  qubit-probes that interact with the protons near them, considered as the environment.

The experiments are carried out at a high magnetic field, as the Zeeman energy is  $\gtrsim 10^5$  times stronger than the spin-spin interactions. Thus only the secular part of the internuclear dipolar Hamiltonian contributes to the dynamics [52]. Therefore the full Hamiltonian of the system is

$$H = H_S + H_E + H_{SE}, \quad (\text{A.15})$$

where the qubit-probe (carbon) considered as our system  $S$ , the environment (protons) and the system-environment interaction Hamiltonians are

$$\begin{aligned} H_S &= \gamma_C B_0 S_z \otimes \mathbb{I}_E + \text{control}, \\ H_E &= \gamma_H B_0 \mathbb{I}_S \otimes I_z + \sum_{i \neq j} d_{ij}^H (2I_z^i I_z^j - I_x^i I_x^j - I_y^i I_y^j) + \text{control}, \\ H_{SE} &= S_z \sum_i d_i I_z^i = S_z B, \end{aligned}$$

respectively.

Here, the sums run over the environmental spins (the protons),  $\gamma_C$  and  $\gamma_H$  are the gyromagnetic ratios of the  $^{13}\text{C}$  and proton, respectively,  $B_0$  is the static field applied in the  $z$ -direction, the spin operators  $\mathbf{S}$  is the qubit-probe ( $^{13}\text{C}$  spin) and  $\mathbf{I}^i$  are the environmental spins with  $\mathbf{I} = \sum_i \mathbf{I}^i$  the total spin moment of the environment,  $d_{ij}^H$  are the dipolar couplings between the environmental spins  $i$  and  $j$ ,  $d_i$  is the dipolar coupling between the qubit-probe and the  $i$ -th spin of the environment. The noise operator is  $B = \sum_i d_i I_z^i$  that represents the field that the qubit-probe experiences due to the environment.

In the interaction picture with respect to the Zeeman interactions, the Hamiltonians become [52]

$$\begin{aligned} H_S &= \text{control}, \\ H_E &= \sum_{i \neq j} d_{ij}^H (2I_z^i I_z^j - I_x^i I_x^j - I_y^i I_y^j) + \text{control}, \\ H_{SE} &= S_z \sum_i d_i I_z^i = S_z B. \end{aligned}$$

We utilize control over the environment solely to create the nonstationary initial state. Subsequently, during the quantum simulations of the SENSIT protocol, only the qubit-probe is controlled. For our experiments, we applied on-resonance  $\pi$ -pulses with the qubit-probe. In the interaction picture with respect to this control, i.e. the toggling frame [53], the Hamiltonian is

$$\begin{aligned} H_S &= 0, \\ H_E &= \sum_{i \neq j} d_{ij}^H (2I_z^i I_z^j - I_x^i I_x^j - I_y^i I_y^j), \\ H_{SE} &= f(t) S_z \sum_i d_i I_z^i = f(t) S_z B, \end{aligned}$$

where the function  $f(t)$ , switches its signs whenever a  $\pi$ -pulse is applied [4].

These Hamiltonians have time-reversal symmetry. To write this explicitly, we use the representation  $I_\alpha^i = \frac{1}{2}\sigma_\alpha^i$ ,  $S_z = \frac{1}{2}\sigma_\alpha^S$ , where  $\sigma_\alpha^i$  are Pauli matrices that act on the space of the  $i$ -th environment spin and  $\sigma_\alpha^S$  are Pauli matrices that act on the qubit space. The time reversal operator is

$$T = \sigma_y^S \prod_i \sigma_y^i K, \quad (\text{A.17})$$

where  $K$  is the complex conjugation operator [38]. Since the system is at high temperature, the contribution of non-commutation terms to the SENSIT contrast will be negligible, thus any measured SENSIT contrast is due to asymmetry generated by the environment initial state. In particular, if the state commutes with the environmental Hamiltonian and has time-reversal symmetry, then the system will have time-reversal symmetry in the control functions.

To finally obtain a Hamiltonian with the form of Eq. (1) in the main text, we switch to an interaction picture with respect to the environmental Hamiltonian

$$H(t) = H_{SE}(t) = f(t) S_z B(t),$$

where  $B(t) = e^{iH_E t} B e^{-iH_E t}$  is the time-dependent noise operator. This is the experimental implementation of Eq. (1) of the main text in our quantum simulations.

## 2. Out-of-equilibrium environmental-state preparation

In this section we describe the pulse sequence used in the experiments described in Fig. 4. For the quantum simulations, we first need to prepare an out-of-equilibrium environment state of the form

$$\rho_0 = S_x \otimes \rho_E,$$

with  $[\rho_E, H_E] \neq 0$ . Before this preparation, the initial state of the full system is in a Boltzmann thermal equilibrium state. Since the experiments were conducted at room temperature, and the Zeeman energy is  $\lesssim 15000$  times lower than the thermal energy, the state is described in the high temperature limit [52]. Therefore, the initial state is  $\rho \simeq \frac{1}{\text{tr}[\mathbb{I}]} (\mathbb{I} - \beta H)$ . As the Zeeman coupling to the external magnetic field is dominant over the dipolar coupling between nuclei, the state is further simplified  $\rho \simeq \frac{1}{\text{tr}[\mathbb{I}]} [\mathbb{I} - \beta \gamma_C B_0 S_z \otimes \mathbb{I}_E - \beta \gamma_H B_0 \mathbb{I}_S \otimes I_z]$ . The initial step in the experiments involves performing cross-polarization between the environment (the protons) and the qubit (the carbons) just to increase the nuclear polarization of the carbons, and thus improve the signal-to-noise ratio of the qubit-probe signal by a factor of  $\gamma_H/\gamma_C \simeq 3.97$ . Then to remove any possible correlation between the carbons and protons, we store the qubit (carbon) magnetization in the  $z$  direction and wait 10ms (time longer than  $T_2$  of both spin species) to scramble out any proton signal and carbon-proton correlations. This process is shown in the Qubit-Sensor Initialization block of Fig. 4. The  $\frac{\pi}{2}$  pulse durations we used for the protons and carbons were  $3.4\mu\text{s}$  and  $5.5\mu\text{s}$ , respectively. The duration of the carbon  $\pi$  pulses was  $11\mu\text{s}$ . After this we apply a  $(\pi/2)_y$ -pulse on the qubit-probe around the  $y$ -axis, to obtain the state of the qubit-environment system  $\rho \simeq \frac{1}{\text{tr}[\mathbb{I}]} [\mathbb{I} - \beta \gamma_H B_0 S_x \otimes \mathbb{I}_E]$ . We can thus write the state of our system just before the preparation time period as  $\rho = (\frac{1}{2} + \tilde{p} S_x) \otimes \frac{\mathbb{I}_E}{\text{tr}[\mathbb{I}_E]}$ , a separable state where the environment is at infinite temperature and the qubit-probe is polarized in the  $x$  direction. Here the polarization of the qubit is  $\tilde{p} = \beta \gamma_H B_0$ . Hereafter, we drop the term  $\frac{1}{2} \otimes \frac{\mathbb{I}_E}{\text{tr}[\mathbb{I}_E]}$ , since it does not contribute to the qubit-probe signal, and we get

$$\rho = \tilde{p} S_x \otimes \frac{\mathbb{I}_E}{\text{tr}[\mathbb{I}_E]}, \quad (\text{A.18})$$



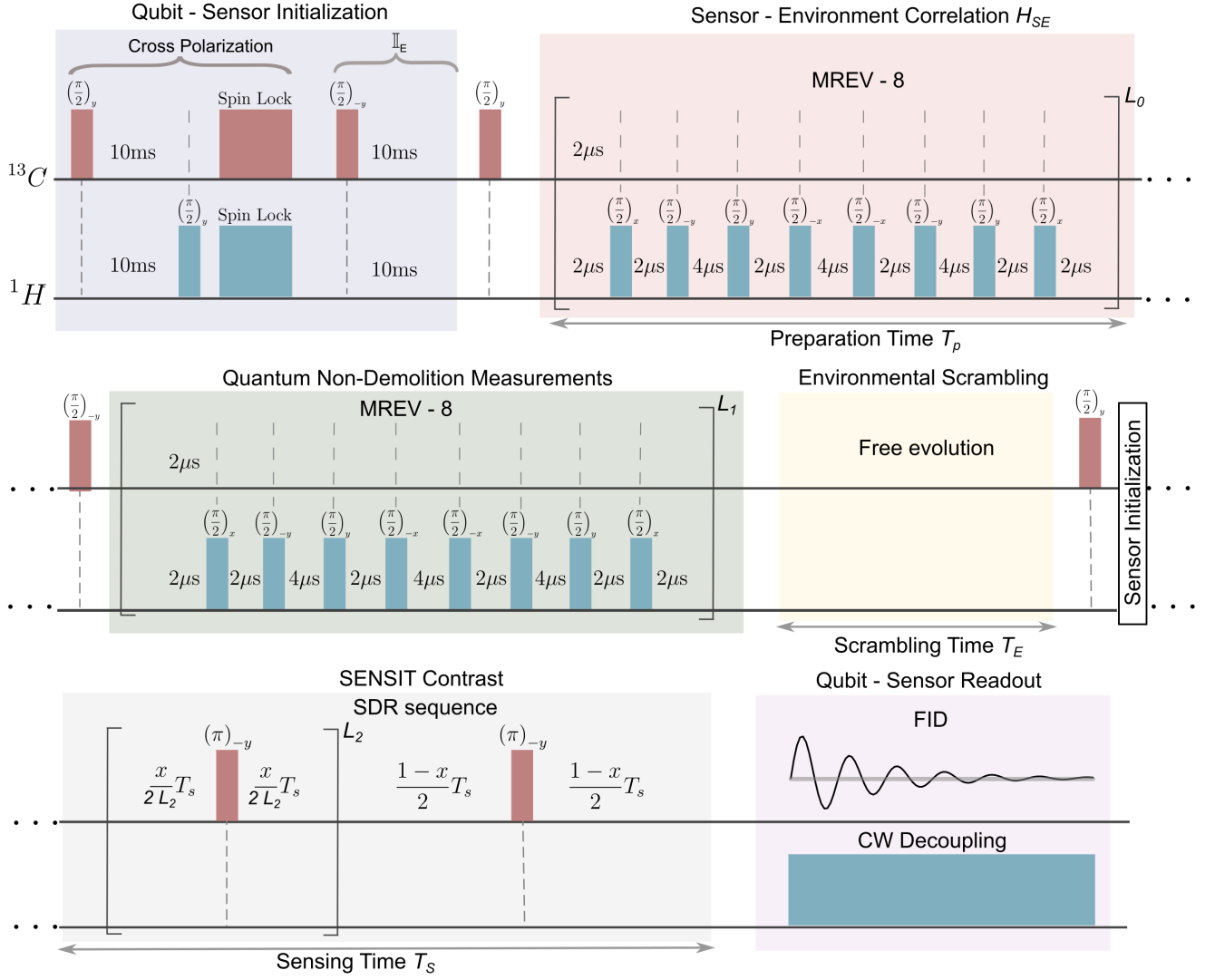


Figure 4. Pulse sequence used for the SENSIT experiments. The different blocks represents different conceptual steps. First, cross polarization is used to initialize the system and increase the signal-to-noise ratio. Then, the 10ms delay time ensures that all qubit-environment correlations and environmental initial state are erased due to  $T_2$  relaxation before further control. This is then followed by a  $(\pi/2)_y$  pulse, to put the qubit-probe state in-plane. Then  $L_0$  cycles of the MREV-8 sequence are implemented to correlate the qubit-probe and the environment and a  $(\pi/2)_{-y}$  pulse returns the qubit-probe state to the  $z$  direction. The preparation time  $T_p$  is the total duration of the  $L_0$  MREV-8 cycles. After that, the MREV-8 sequence is used again to mimic a projective measurement on the qubit-probe and turn the correlated state into a state where the qubit and environment are uncorrelated, but with the environment out of equilibrium. To ensure the completeness of the projective measurement, we attain a stationary state by varying  $L_1$ . Specifically, we set  $L_1 = 42$  because for larger values, the qubit-probe state remained unchanged despite alterations in  $L_1$ . The environment is then scrambled by letting it evolve freely during an environmental scrambling time  $T_E$ . The qubit-probe state is then put in plane with a  $(\pi/2)_y$  pulse, and the SDR sequence is applied during the sensing time  $T_s$  to sense the environment via the readout of the qubit-probe state. During this readout, the environment is decoupled for improving the signal-to-noise ratio using continuous wave decoupling. To obtain the SENSIT contrast the experiment is repeated exchanging the SDR sequence by the TSDR sequence.

The environmental state  $\frac{\mathbb{I}_E}{\text{tr}[\mathbb{I}_E]}$  is proportional to the identity and thus it is invariant under the time reversal operation of Eq. (A.17), and it also commutes with the environmental Hamiltonian. Since the experiments are carried out at high temperature (See SI G 1), if the environmental state  $\rho_E$  is stationary and invariant under time reversal, then the conditions outlined in SI C are satisfied, indicating that the system possesses time-reversal symmetry in the qubit-probe control functions. We therefore predict to observe a null SENSIT contrast when the environment is in this state.

Then to turn this state into an out-of-equilibrium state, we perform the following preparation step. We apply the MREV-8 pulse sequence [54] during the preparation time  $T_p$  on the environmental spins to decouple them, i.e. cancel out the dipole-dipole interaction between them thus making null the environmental Hamiltonian. We used a MREV cycle time of 54, 4  $\mu$ s. This is shown in Fig. 4, in the block labeled Sensor-Environment Correlation  $H_{SE}$ . The effective full system Hamiltonian  $H$  in the rotating frame of both the qubit-probe and the environmental spins (i.e., in the interaction picture with respect to the Zeeman Hamiltonians) is solely the interaction Hamiltonian  $H_{SE}$ , with the field  $B$  fixed in time as the evolution stemming from the environmental Hamiltonian is refocused by the MREV sequence

$$H_{SE} = S_z \sum_i d_i I_z^i = S_z B.$$

During this step the qubit dephases due to interaction with the environment. The full qubit-environment state becomes  $\rho(T_p) = \tilde{p} e^{-iS_z B T_p} \left( \frac{1}{2} + \tilde{p} S_x \right) \otimes \frac{\mathbb{I}_E}{\text{tr}[\mathbb{I}_E]} e^{iS_z B T_p}$ , or equivalently

$$\rho(T_p) = \tilde{p} \left( S_x \otimes \frac{\cos(BT_p)}{\text{tr}[\mathbb{I}_E]} + S_y \otimes \frac{\sin(BT_p)}{\text{tr}[\mathbb{I}_E]} \right). \quad (\text{A.19})$$

As this state is not separable, we have created quantum correlations between the environmental spins and the qubit-probe. This is simply a free induction decay due to the constant but random field  $B$  felt by the qubit-probe.

We then proceeded to erase the qubit-environment correlations mimicking a quantum non-demolition (QND) measurement on the qubit-probe, while maintaining the non-equilibrium status of the environmental state to attain a state like the one described in Eq. (A.1). To do this, we apply a  $(\pi/2)_{-y}$ -pulse around the  $-y$  direction, and get the state

$$\tilde{p} \left[ S_z \otimes \frac{\cos(BT_p)}{\text{tr}[\mathbb{I}_E]} + S_y \otimes \frac{\sin(BT_p)}{\text{tr}[\mathbb{I}_E]} \right].$$

The first term satisfies  $\left[ S_z \otimes \frac{\cos(BT_p)}{\text{tr}[\mathbb{I}_E]}, H_{SE} \right] = 0$  and thus does not evolve, but the second one does evolve, and it will be dephased—vanished—due to the interaction with the environmental field  $B$ . We thus apply the MREV-8 sequence for a sufficient duration to dephase the second term, effectively simulating a quantum non-demolition (QND) measurement on the qubit-probe state, where the state is projected onto the subspace proportional to  $S_z$ . This is shown in the Quantum Non-Demolition Measurements block in Fig. 4. As long as we do not refocus this dephasing with a time-reversion, the qubit-probe signal we measure only comes from the state  $\tilde{p} S_z \otimes \frac{\cos(BT_p)}{\text{tr}[\mathbb{I}_E]}$ .

For the experiments described in Fig. 3 of the main text, this is the step where environmental scrambling is introduced. During the scrambling time  $T_E$  a waiting period is introduced without applying the MREV-8 sequence, as shown in Fig. 4 within the Environmental Scrambling block, so the environment Hamiltonian produces the information scrambling on the environmental state. The created state is thus  $\tilde{p} S_z \otimes e^{-iH_E T_E} \frac{\cos(BT_p)}{\text{tr}[\mathbb{I}_E]} e^{iH_E T_E}$ . This scrambling step is skipped for the experiments of Fig. 2.

Finally we apply a last  $(\pi/2)_y$ -pulse (Fig. 4, Sensor Initialization), and obtain when the scrambling time is included on the sequence

$$\rho_0 = \tilde{p} S_x \otimes e^{-iH_E T_E} \frac{\cos(BT_p)}{\text{tr}[\mathbb{I}_E]} e^{iH_E T_E}.$$

This state is again separable, but it does not commute with the environment Hamiltonian, as  $[B, H_E] \neq 0$ , and thus it is now in an out-of-equilibrium state that produces non-stationary noise fluctuations on the qubit-probe. Thus, we rewrite this as

$$\rho_0 = p S_x \otimes \rho_E,$$

where  $p = \tilde{p} \frac{\text{tr}[\cos(BT_p)]}{\text{tr}[\mathbb{I}_E]}$  is the initial qubit-probe polarization for the sensing process, and  $\rho_E = e^{-iH_E T_E} \frac{\cos(BT_p)}{\text{tr}[\cos(BT_p)]} e^{iH_E T_E}$  is the out-of-equilibrium environmental density matrix. In experiments of Fig. 2, without including the scrambling time, the environmental state is  $\rho_E = \frac{\cos(BT_p)}{\text{tr}[\cos(BT_p)]}$ . Again, since  $[B, H_E] \neq 0$  this state is nonstationary. This shows how the initial out-of-equilibrium state is prepared in our experiments.

The last step of the pulse sequence measures the SENSIT contrast. In our experiments, we applied the selective dynamical recoupling (SDR) sequence [40, 41], which is based on a dynamical decoupling sequences that is asymmetric under time-reversal, thus satisfying the requirements for obtaining nonzero SENSIT contrasts. Figure 4 shows the SDR implementation of the sequence in the SDR sequence block. We used 12 pulses and a total sensing time of  $T_s = 750 \mu$ s for the experiments of Fig. 2 and 3. To measure the SENSIT contrast we also applied the time reversed version of SDR, the TSDR sequence, by reversing the order in which the pulses and delays are applied. The SDR sequence interpolates

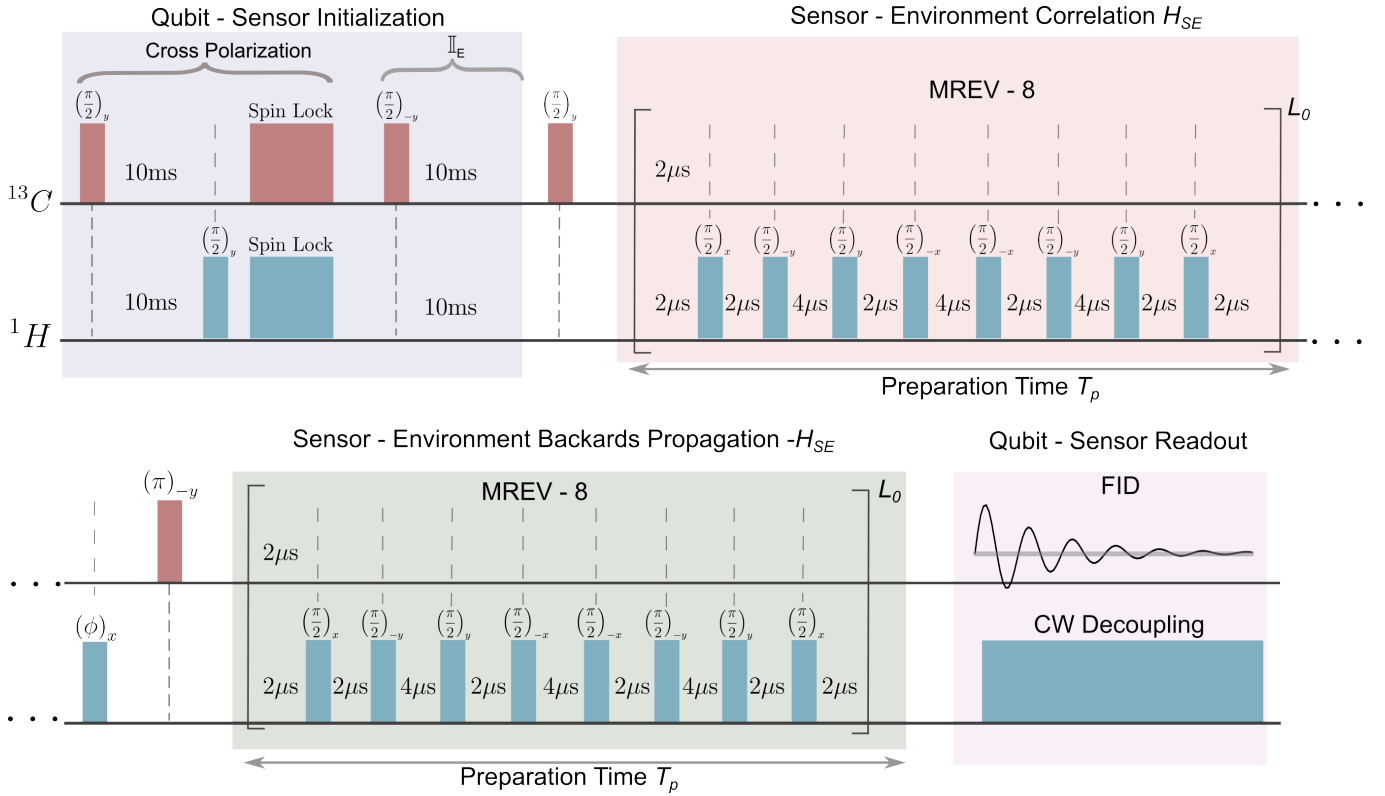


Figure 5. Pulse sequence used to measure the number  $K$  of environmental spins correlated to the qubit-sensor. First, cross polarization is used to initialize the system and increase the signal-to-noise ratio. Then, the 10ms delay time ensures that all qubit-environment correlations and environmental initial state are erased due to  $T_2$  relaxation before further control. This is followed by a  $(\pi/2)_y$  pulse, putting the qubit-probe state in plane. Then  $L_0$  cycles of the MREV-8 sequence are implemented to correlate the qubit-probe and the environment, as done when measuring the SENSIT contrast. After this, a  $(\phi)_x$  pulse is applied on the environment to encode the formed correlations [46]. Then an time-reversal echo is created by means of a  $(\pi)_{-y}$  pulse on the qubit-probe followed by  $L_0$  cycles of the MREV-8 sequence to produce an effective backwards evolution. Finally the qubit-probe state is read out, while it is decoupled from the environment with continuous wave irradiation for improving the signal-to-noise ratio.

continuously a Hahn echo sequence of duration  $T_s$  with a CPMG sequence consisting of  $N$  equidistant  $\pi$  pulses between  $t = 0$  and  $t = T_s$ . It consists of  $N - 1$  equidistant  $\pi$  pulses between  $t = 0$  and  $t = xT_s$  and a last  $\pi$  pulse at  $\frac{x+1}{2}T_s$ . The dimensionless parameter  $x$  of the sequence interpolates the sequence between the Hahn echo at  $x = 0$  and the CPMG sequence of  $N$  pulses at  $x = \frac{N-1}{N}$ . It can be interpreted as concatenating  $N - 1$  spin echoes of duration  $\frac{x}{N-1}T_s$ , and a last single spin echo of duration  $(1 - x)T_s$ . For the time-reversed version TSDR, one first applies the single spin echo of duration  $(1 - x)T_s$ , and then concatenates the  $N - 1$  spin echoes of duration  $\frac{x}{N-1}T_s$ . The two different sequences are shown side by side in Fig. 2 of the main text. Finally, the signal of the qubit-probe after the SDR and TSDR sequences is measured under CW decoupling being applied to the protons to increase the signal-to-noise ratio (Fig. 4, Qubit-Sensor Readout).

The SENSIT contrast vanishes for  $T_p = 0$  as the system is in the state described in Eq. (A.18). As the preparation time  $T_p$  increases, the state is driven further away from equilibrium, leading to a growth in the nonstationary contributions to the cumulants. Therefore, a growth of the SENSIT contrast is expected with increasing  $T_p$ , as shown in Fig. 2c of the main text. If the scrambling time  $T_E$  is included, we anticipate a decrease in the SENSIT contrast with increasing  $T_E$ . This is because the local information about the nonstationary state becomes increasingly scrambled in nonlocal degrees of freedom that are not accessible from the sensor qubit. This phenomenon is shown in Fig. 3 of the main text.

### 3. Quantifying the number $K$ of correlated spins in the Environment due to initial state preparation

As we use the qubit-probe as a resource to create the out-of-equilibrium state in the environment, by driven correlations between the qubit and environmental spins, we measure the number of correlated environmental spins as a measure of

the out-of-equilibrium degree. We use the method developed in [55] to measure the multiple-quantum coherence (MQC) spectrum of the density matrix state. Based on this approach the second moment of the MQC spectrum gives an out-of-time-order commutator  $K$  that quantifies the number of correlated spins where the information was scrambled from a local probe [13, 43, 46, 56]. Given that the nonstationary state post-preparation arises from correlations established between the qubit-sensor and the environment, the out-of-time-order commutator  $K$  serves as an indicator of the system's distance from equilibrium.

To measure the number of correlated spins  $K$  we begin with the same initialization as for the experiments to measure the SENSIT contrast: A cross polarization followed by a dephasing of correlations (see Fig. 5, Qubit-Sensor Initialization). We then correlate the qubit and the environment in the same way as done when measuring the SENSIT contrast: we apply a  $(\pi/2)_y$  pulse to put the qubit-probe state in plane, then apply  $L_0$  cycles of the MREV-8 pulse sequence to create a state where the qubit-probe and environment are correlated (see Fig. 5, Sensor-Environment Correlation  $H_{SE}$ ). This creates the correlated state described in Eq. (A.19). We then apply a rotation pulse  $e^{i\phi I_x}$  on the environment spins by an angle  $\phi$  around the  $x$  direction. To then create a time-reversal echo, we apply a  $\pi$ -pulse on the qubit-probe to effectively change the sign of the system-environment Hamiltonian that creates the correlations, and apply again the MREV-8 sequence during a time  $T_p$  (see Fig. 5, Sensor-Environment Backwards Propagation  $-H_{SE}$ ). This last step effectively creates a backward evolution to refocus the initial state. After that, a time reversal echo is created whose amplitude depends on  $\phi$  to allow encoding the number of correlated spins  $K$  [13, 43, 46, 56]. Finally, the amplitude of the echo is measured, as shown in Fig. 5, Qubit-Sensor Readout.

The total evolution operator of this time reversal quantum evolution is thus  $U_{\text{echo}} = e^{iS_z B T_p} e^{i\phi I_x} e^{-iS_z B T_p}$ . The density matrix of Eq. (A.19) can be written as  $\rho(T_p) = \sum_M \rho_M$ , where  $\rho_M$  are the multiple-quantum coherence blocks of order  $M$ , defined by the property  $e^{i\phi I_x} \rho_M e^{-i\phi I_x} = e^{i\phi M} \rho_M$ . The effect of rotating the environmental spins around the  $x$  axis thus adds a different phase to each coherence component  $\rho_M$  of the density matrix, i.e.  $e^{i\phi I_x} \rho(T_p) e^{-i\phi I_x} = \sum_M e^{i\phi M} \rho_M$ . The measured echo is therefore

$$\langle \rho_0 U_{\text{echo}} \rho_0 U_{\text{echo}}^\dagger \rangle = \langle \rho(T_p) e^{i\phi I_x} \rho(T_p) e^{-i\phi I_x} \rangle = \sum_M e^{i\phi M} \langle \rho_M^\dagger \rho_M \rangle.$$

The dependence of this measured echo with respect to  $\phi$  encodes the MQC spectrum  $\langle \rho_M^\dagger \rho_M \rangle$ , as they are multiplied by  $e^{i\phi M}$ . The Fourier transform of the echo signal with respect to the phase  $\phi$  is the MQC spectrum  $\langle \rho_M^\dagger \rho_M \rangle$ . The effective number of correlated spins  $K$  is determined from the width of the MQC spectrum, i.e. its second moment  $K = \frac{\sum_M M^2 \langle \rho_M^\dagger \rho_M \rangle^2}{\sum_M \langle \rho_M^\dagger \rho_M \rangle^2} = \langle [\rho, I_x]^\dagger [\rho, I_x] \rangle$ , where  $\sum_M \langle \rho_M^\dagger \rho_M \rangle = \text{tr} \rho^2$  is constant [13, 43, 46, 56]. The second moment  $K$  quantifies the norm of the commutator between the localized initial state before the preparation time with the evolved density matrix after the preparation time [43, 56]. This thus determine a measure of distance to equilibrium based on the number of correlated spins. Notice that this state does not commute with the equilibrium state, thus relaxes to equilibrium during the scrambling time.

---

\* [gonzalo.alvarez@conicet.gov.ar](mailto:gonzalo.alvarez@conicet.gov.ar)

- [1] [Awschalom, Hanson, Wrachtrup, and Zhou]D. D. Awschalom, R. Hanson, J. Wrachtrup, and B. B. Zhou, *Nat. Photonics* **12**, 516 (2018).
- [2] A. Acín, I. Bloch, H. Buhrman, T. Calarco, C. Eichler, J. Eisert, D. Esteve, N. Gisin, S. J. Glaser, F. Jelezko, S. Kuhr, M. Lewenstein, M. F. Riedel, P. O. Schmidt, R. Thew, A. Wallraff, I. Walmsley, and F. K. Wilhelm, *New J. Phys.* **20**, 080201 (2018).
- [3] E. Pelucchi, G. Fagas, I. Aharonovich, D. Englund, E. Figueroa, Q. Gong, H. Hannes, J. Liu, C.-Y. Lu, N. Matsuda, J.-W. Pan, F. Schreck, F. Sciarrino, C. Silberhorn, J. Wang, and K. D. Jöns, *Nat. Rev. Phys.* **4**, 194 (2022).
- [4] D. Suter and G. A. Álvarez, *Rev. Mod. Phys.* **88**, 041001 (2016).
- [5] C. L. Degen, F. Reinhard, and P. Cappellaro, *Rev. Mod. Phys.* **89**, 035002 (2017).
- [6] N. Aslam, H. Zhou, E. K. Urbach, M. J. Turner, R. L. Walsworth, M. D. Lukin, and H. Park, *Nat. Rev. Phys.* **5**, 157 (2023).
- [7] A. Zwick and G. A. Álvarez, *Journal of Magnetic Resonance Open* **16-17**, 100113 (2023).
- [8] J. F. Barry, M. J. Turner, J. M. Schloss, D. R. Glenn, Y. Song, M. D. Lukin, H. Park, and R. L. Walsworth, *PNAS* **113**, 14133 (2016).
- [9] L. Nie, A. C. Nusantara, V. G. Damle, R. Sharmin, E. P. P. Evans, S. R. Hemelaar, K. J. van der Laan, R. Li, F. P. Perona Martinez, T. Vedelaar, M. Chipaux, and R. Schirhagl, *Sci. Adv.* **7** (2021).
- [10] I. Lovchinsky, A. O. Sushkov, E. Urbach, N. P. de Leon, S. Choi, K. De Greve, R. Evans, R. Gertner, E. Bersin, C. Muller, L. McGuinness, F. Jelezko, R. L. Walsworth, H. Park, and M. D. Lukin, *Science* **351**, 836 (2016).
- [11] L. Schlipf, T. Oeckinghaus, K. Xu, D. B. R. Dasari,



- A. Zappe, F. F. de Oliveira, B. Kern, M. Azarkh, M. Drescher, M. Ternes, K. Kern, J. Wrachtrup, and A. Finkler, *Science Advances* **3**, e1701116 (2017).
- [12] P. Neumann, I. Jakobi, F. Dolde, C. Burk, R. Reuter, G. Waldherr, J. Honert, T. Wolf, A. Brunner, J. H. Shim, D. Suter, H. Sumiya, J. Isoya, and J. Wrachtrup, *Nano Lett.* **13**, 2738 (2013).
- [13] G. A. Álvarez, D. Suter, and R. Kaiser, *Science* **349**, 846 (2015).
- [14] B. Buča, J. Tindall, and D. Jaksch, *Nat. Commun.* **10**, 1730 (2019).
- [15] R. J. Lewis-Swan, A. Safavi-Naini, A. M. Kaufman, and A. M. Rey, *Nat. Rev. Phys.* **1**, 627 (2019).
- [16] K. A. Landsman, C. Figgatt, T. Schuster, N. M. Linke, B. Yoshida, N. Y. Yao, and C. Monroe, *Nature* **567**, 61 (2019).
- [17] T. Chalermputitarak, B. Tonekaboni, Y. Wang, L. M. Norris, L. Viola, and G. A. Paz-Silva, *PRX Quantum* **2**, 030315 (2021).
- [18] M. Kuffer, A. Zwick, and G. A. Álvarez, *PRX Quantum* **3**, 020321 (2022).
- [19] S. Kotler, N. Akerman, Y. Glickman, and R. Ozeri, *Phys. Rev. Lett.* **110**, 110503 (2013).
- [20] L. M. Norris, G. A. Paz-Silva, and L. Viola, *Phys. Rev. Lett.* **116**, 150503 (2016).
- [21] Y. Sung, F. Beaudoin, L. M. Norris, F. Yan, D. K. Kim, J. Y. Qiu, U. von Lüpke, J. L. Yoder, T. P. Orlando, S. Gustavsson, L. Viola, and W. D. Oliver, *Nat. Commun.* **10**, 3715 (2019).
- [22] P. Wang, C. Chen, X. Peng, J. Wrachtrup, and R.-B. Liu, *Phys. Rev. Lett.* **123**, 050603 (2019).
- [23] Y.-X. Wang and A. A. Clerk, *Phys. Rev. Res.* **2**, 033196 (2020).
- [24] Y.-X. Wang and A. A. Clerk, *Nat. Commun.* **12**, 6528 (2021).
- [25] P. C. Jerger, Y.-X. Wang, M. Onizhuk, B. S. Soloway, M. T. Solomon, C. Egerstrom, F. J. Heremans, G. Galli, A. A. Clerk, and D. D. Awschalom, *PRX Quantum* **4**, 040315 (2023).
- [26] G. A. Álvarez and D. Suter, *Phys. Rev. Lett.* **107**, 230501 (2011).
- [27] J. Bylander, S. Gustavsson, F. Yan, F. Yoshihara, K. Harrabi, G. Fitch, D. G. Cory, Y. Nakamura, J. Tsai, and W. D. Oliver, *Nat. Phys.* **7**, 565 (2011).
- [28] Y. Romach, C. Müller, T. Uden, L. J. Rogers, T. Isoda, K. M. Itoh, M. Markham, A. Stacey, J. Meijer, S. Pezzagna, B. Naydenov, L. P. McGuinness, N. Bar-Gill, and F. Jelezko, *Phys. Rev. Lett.* **114**, 017601 (2015).
- [29] D. Schmid-Lorch, T. Häberle, F. Reinhard, A. Zappe, M. Slota, L. Bogani, A. Finkler, and J. Wrachtrup, *Nano Lett.* **15**, 4942 (2015).
- [30] W.-L. Ma, G. Wolfowicz, N. Zhao, S.-S. Li, J. J. L. Morton, and R.-B. Liu, *Nat. Commun.* **5**, 4822 (2014).
- [31] E. J. Connors, J. Nelson, L. F. Edge, and J. M. Nichol, *Nat. Commun.* **13**, 940 (2022).
- [32] J. T. Muhonen, J. P. Dehollain, A. Laucht, F. E. Hudson, R. Kalra, T. Sekiguchi, K. M. Itoh, D. N. Jamieson, J. C. McCallum, A. S. Dzurak, and A. Morello, *Nat. Nanotechnol.* **9**, 986 (2014).
- [33] V. M. Frey, S. Mavadia, L. M. Norris, W. de Ferranti, D. Lucarelli, L. Viola, and M. J. Biercuk, *Nat. Commun.* **8**, 2189 (2017).
- [34] L. Viola, E. Knill, and S. Lloyd, *Phys. Rev. Lett.* **82**, 2417 (1999).
- [35] Y. Sagi, I. Almog, and N. Davidson, *Phys. Rev. Lett.* **105**, 053201 (2010).
- [36] F. K. Malinowski, F. Martins, Ł. Cywiński, M. S. Rudner, P. D. Nissen, S. Fallahi, G. C. Gardner, M. J. Manfra, C. M. Marcus, and F. Kuemmeth, *Phys. Rev. Lett.* **118**, 177702 (2017).
- [37] G. d. Lange, Z. H. Wang, D. Ristè, V. V. Dobrovitski, and R. Hanson, *Science* **330**, 60 (2010).
- [38] B. A. Bernevig and T. L. Hughes, *Topological Insulators and Topological Superconductors* (Princeton University Press, 2013).
- [39] T. Nakajima, A. Noiri, J. Yoneda, M. R. Delbecq, P. Stano, T. Otsuka, K. Takeda, S. Amaha, G. Allison, K. Kawasaki, A. Ludwig, A. D. Wieck, D. Loss, and S. Tarucha, *Nat. Nanotechnol.* **14**, 555 (2019).
- [40] P. E. S. Smith, G. Bensky, G. A. Álvarez, G. Kurizki, and L. Frydman, *PNAS* **109**, 5958 (2012).
- [41] G. A. Álvarez, N. Shemesh, and L. Frydman, *Phys. Rev. Lett.* **111**, 080404 (2013).
- [42] S. Xu and B. Swingle, *PRX Quantum* **5**, 010201 (2024).
- [43] F. D. Domínguez, M. C. Rodríguez, R. Kaiser, D. Suter, and G. A. Álvarez, *Phys. Rev. A* **104**, 012402 (2021).
- [44] J. Li, R. Fan, H. Wang, B. Ye, B. Zeng, H. Zhai, X. Peng, and J. Du, *Phys. Rev. X* **7**, 031011 (2017).
- [45] M. Gärttner, P. Hauke, and A. M. Rey, *Phys. Rev. Lett.* **120**, 040402 (2018).
- [46] M. Niknam, L. F. Santos, and D. G. Cory, *Phys. Rev. Res.* **2**, 013200 (2020).
- [47] S. Li, L. Lu, S. Bhattacharyya, C. Pearce, K. Li, E. T. Nienhuis, G. Doumy, R. D. Schaller, S. Moeller, M.-F. Lin, G. Dakovski, D. J. Hoffman, D. Garratt, K. A. Larsen, J. D. Koralek, C. Y. Hampton, D. Cesar, J. Duris, Z. Zhang, N. Sudar, J. P. Cryan, A. Marinelli, X. Li, L. Inhester, R. Santra, and L. Young, *Science* **383**, 1118 (2024).
- [48] A. Greilich, N. E. Kopteva, A. N. Kamenskii, P. S. Sokolov, V. L. Korenev, and M. Bayer, *Nat. Phys.* **1**, 1 (2024).
- [49] S. K. Sridhar, S. Ghosh, D. Srinivasan, A. R. Miller, and A. Dutt, *Nat. Phys.* **1**, 1 (2024).
- [50] T. Shimasaki, M. Prichard, H. E. Kondakci, J. E. Pagett, Y. Bai, P. Dotti, A. Cao, A. R. Dardia, T.-C. Lu, T. Grover, and D. M. Weld, *Nat. Phys.* **20**, 409 (2024).
- [51] N. G. van Kampen, *Stochastic Processes in Physics and Chemistry* (Elsevier Science Publishers, Amsterdam, 1992).
- [52] C. Slichter, *Principles of Magnetic Resonance* (Springer Berlin Heidelberg, Berlin, Heidelberg, 1996).
- [53] A. Abragam, *Principles of Nuclear Magnetism*, International Series of Monographs on Physics (Oxford University Press, Oxford, New York, 1983).
- [54] W. K. Rhim, D. D. Elleman, and R. W. Vaughan, *J. Chem. Phys.* **58**, 1772 (1973).
- [55] J. Baum, M. Munowitz, A. N. Garroway, and A. Pines, *J. Chem. Phys.* **83**, 2015 (1985).
- [56] F. D. Domínguez and G. A. Álvarez, *Phys. Rev. A* **104**, 062406 (2021).